SYNTHESIS OF POLY(DL-LACTIC-CO-GLYCOLIC ACID) COATED MAGNETIC NANOPARTICLES FOR ANTI-CANCER DRUG DELIVERY

A THESIS SUBMITTED TO
THE GRADUATE SCHOOL OF NATURAL AND APPLIED SCIENCES
OF
MIDDLE EAST TECHNICAL UNIVERSITY

BY

GÜLİSTAN TANSIK

IN PARTIAL FULFILLMENT OF THE REQUIREMENTS
FOR
THE DEGREE OF MASTER OF SCIENCE
IN
BIOLOGY

FEBRUARY 2012

Approval of the thesis:

SYNTHESIS OF POLY(DL-LACTIC-CO-GLYCOLIC ACID) COATED MAGNETIC NANOPARTICLES FOR ANTI-CANCER DRUG DELIVERY

submitted by **GÜLİSTAN TANSIK** in partial fulfillment of the requirements for the degree of **Master of Science in Biology Department, Middle East Technical University** by,

Prof. Dr. Canan Özgen _____
Dean, Graduate School of **Natural and Applied Sciences**

Prof. Dr. Musa Doğan _____
Head of Department, **Biology**

Prof. Dr. Ufuk Gündüz
Supervisor, **Biology Dept., METU** _____

Examining Committee Members:

Assoc.Prof.Dr. Ayşen Tezcaner _____
Engineering Sci. Dept., METU

Prof. Dr. Ufuk Gündüz _____
Biology Dept., METU

Assist. Prof. Dr. Sreeparna Banerjee _____
Biology Dept., METU

Assist. Prof. Dr.Çağdaş Son _____
Biology Dept., METU

Assist. Prof. Dr.Arzu Yakar _____
Chemical Eng. Dept., AKU

Date: 10.02.2012

I hereby declare that all information in this document has been obtained and presented in accordance with academic rules and ethical conduct. I also declare that, as required by these rules and conduct, I have fully cited and referenced all material and results that are not original to this work.

Name, Last name: GÜLİSTAN TANSIK

Signature :

ABSTRACT

SYNTHESIS OF POLY(DL-LACTIC-CO-GLYCOLIC ACID) COATED MAGNETIC NANOPARTICLES FOR ANTI-CANCER DRUG DELIVERY

Tansık, Gülistan

M.Sc., Department of Biology

Supervisor: Prof. Dr. Ufuk Gündüz

February 2012, 82 pages

One of the main problems of current cancer chemotherapy is the lack of selectivity of anti-cancer drugs to tumor cells which leads to systemic toxicity and adverse side effects. In order to overcome these limitations, researches on controlled drug delivery systems have gained much attention. Nanoscale based drug delivery systems provide tumor targeting. Among many types of nanocarriers, superparamagnetic nanoparticles with their biocompatible polymer coatings can be targeted to an intented site by an external magnetic field. Thus, the drug can be carried to the targeted site safely.

The aim of this study is to prepare poly(dl-lactic-co-glycolic acid) (PLGA) coated magnetic nanoparticles and load anti-cancer drug, doxorubicin to them. For this purpose, magnetite (Fe_3O_4) iron oxide nanoparticles were synthesized as a magnetic core material (MNP) and then coated with oleic acid. Oleic acid coated MNP (OA-MNP) was encapsulated into PLGA. Effects of different OA-MNP/PLGA ratios on magnetite entrapment efficiency were investigated. Doxorubicin loaded magnetic polymeric nanoparticles (DOX-PLGA-MNP) were prepared. After the characterization of prepared nanoparticles, their cytotoxic effects on MCF-7 cell line were studied.

PLGA coated magnetic nanoparticles (PLGA-MNP) had a proper size and superparamagnetic character. The highest magnetite entrapment efficiency of PLGA-MNP was estimated as 63 % at 1:8 ratio. Cytotoxicity studies of PLGA-MNP did not indicate any notable cell death between the concentration ranges of 2 and 250 μg ml^{-1}. It was observed that DOX-PLGA-MNP showed significant cytotoxicity on MCF-7 cells compared to PLGA-MNP.

The results showed that prepared nanoparticles have desired size and superparamagnetic characteristics without serious toxic effects on cells. These nanoparticles may be suitable for targeted drug delivery applications. The findings obtained from drug studies may contribute to further work.

Keywords: Fe_3O_4, PLGA, Doxorubicin, MCF-7, Targeted Anti-Cancer Drug Delivery

ÖZ

ANTİ-KANSER İLAÇ TAŞINMASINA YÖNELİK POLİ(DL-LAKTİK-KO-GLİKOLİK ASİT) KAPLI MANYETİK NANOPARÇACIKLARIN SENTEZLENMESİ

Tansık, Gülistan
Yüksek Lisans, Biyoloji Bölümü
Tez Yöneticisi: Prof. Dr. Ufuk Gündüz
Şubat 2012, 82 sayfa

Günümüzde kanser kemoterapisinin en önemli sorunlarından biri, kullanılan anti-kanser ilaçlarının kanserli hücreyi ayırt edici özelliğe sahip olmamaları ve yan etki olarak sağlıklı hücrelerin üzerinde de toksik etki göstermeleridir. Bu problemlere çözüm bulmak amacı ile kontrollü ilaç salım sistemleri üzerine yapılan çalışmalar artmıştır. Nanoboyuttaki kontrollü ilaç taşıma sistemleri tümör hedeflenmesine olanak sağlamıştır. Nanotaşıyıcılar arasından, biyouyumlu polimer kaplı süperparamanyetik nanoparçacıklar dışardan uygulanan manyetik alan ile istenilen bölgeye hedeflenebilme özelliklerine sahiptirler. Bu sayede ilaç hedeflenen bölgeye güvenli bir şekilde taşınabilmektedir.

Bu çalışmanın amacı poli(dl-laktik-ko-glikolik asit) (PLGA) kaplı manyetik nanoparçacıkların sentezlenmesi ve onlara anti-kanser ilaç, doksorubisinin

yüklenmesidir. Sentezlenen manyetit (Fe_3O_4) demiroksit parçacıkları manyetik çekirdek olarak kullanılmış ve yüzeyi oleik asit ile kaplanmıştır. Oleik asit ile kaplı manyetik nanoparçacıklar (OA-MNP), PLGA içerisine hapsedilmiştir. Farklı demir/polimer oranlarının polimerin demir bağlama kapasitesi üzerindeki etkisi incelenmiştir. Doksorubisin yüklü polimer kaplı manyetik nanoparçacıklar (DOX-PLGA-MNP) hazırlanmıştır. Elde edilen nanoparçacıkların karakterizasyonu yapıldıktan sonra, MCF-7 hücre hattı üzerindeki sitotoksik etkileri incelenmiştir.

PLGA kaplı manyetik nanoparçacıklar (PLGA-MNP) istenilen boyut ve süperparamanyetik özelliklere sahiptirler. Farklı OA-MNP/PLGA oranları içerisinde en yüksek demir bağlama kapasitesi 1:8 oranı ile % 63 olarak bulunmuştur. Sitotoksisite çalışmalarında, 2-250 $\mu g\ ml^{-1}$ derişim aralığında PLGA-MNP'lerin hücreler üzerinde önemli bir toksik etkisinin olmadığı gözlenmiştir. İlaç yüklenmemiş PLGA-MNP'lerle karşılaştırıldığında, DOX-PLGA-MNP'lerin MCF-7 hücreleri üzerinde ciddi toksik etkiye sahip oldukları görülmüştür.

Elde edilen sonuçlar, manyetik nanoparçacıkların istenilen boyut ve süperparamanyetik özellikte olduklarını ve hücreler üzerinde ciddi toksik etkilerinin olmadığını göstermiştir. Bu özellikleri ile ilaç hedefleme çalışmalarında kullanılabilirler. İlaçla yapılan çalışmalardan elde edilen sonuçlar ileride yapılacak olan çalışmalara katkı sağlayacaktır.

Anahtar kelimeler: Fe_3O_4, PLGA, Doksorubisin, MCF-7, Anti-Kanser İlaç Hedeflemesi

To the memory of my beloved father, Mehmet Tansık,

ACKNOWLEDGEMENTS

Firstly, I would like to express my sincere gratitude to my supervisor Prof. Dr. Ufuk Gündüz for her guidance, motivation, continuous support and invaluable advises throughout my study.

I would like to thank to Prof. Dr. Güngör Gündüz for granting me permission to make experiments in his laboratory and valuable comments on my research.

I am deeply indepted to Assist. Prof. Dr. Arzu Yakar for her endless support and patience throughout this work and, precious contributions and advises to my study.

My special thanks go to Tuğba Keskin, Zelha Nil and Burcu Özsoy for their valuable friendship, support and funny times we have had.

I would like to thank to Dr. Özlem Darcansoy İşeri, Yaprak Dönmez, Petek Şen, Esra Kaplan and Gülşah Pekgöz for sharing their experiences and also for their friendship.

I also would like to thank my lab mates for their friendship and support during my studies in Lab 206 : Çağrı Urfalı, Ahu İzgi, Ruhollah Khodadust, Gözde Ünsoy, Çiğdem Şener, Okan Tezcan, Murat Erdem, Aktan Alpsoy, and Neşe Çakmak.

I gratefully thank to Zeynep Kavalcı for her great contributions in my life throughout this study.

I acknowledge Assist. Prof. Dr. Bora Maviş for his support in FTIR Spectroscopy measurements.

Cengiz Tan is acknowledged for his help to support experiment equipments leading to complete this study.

I owe my deepest gratitude to my family, especially my father Mehmet Tansık, mother Cahide Tansık and brother Ali Erdem Tansık, for their endless support, patience, motivation, trust and love throughout my life. Without them I would not be where I am now.

This study was supported by the Research Funds of METU Grant No: BAP-07-02-2010-00-01 and TUBITAK Grant No: 109T949.

TABLE OF CONTENTS

LIST OF TABLES

TABLES

LIST OF FIGURES

FIGURES

LIST OF ABBREVIATIONS

ACS	American Cancer Society
BT	Body temperature
dH_2O	Deionized water
DCM	Dichloromethane
DMSO	Dimethyl sulfoxide
DOX	Doxorubicin
DOX-PLGA-MNP	Doxorubicin loaded magnetic polymeric nanoparticle
EE	Encapsulation efficiency
FBS	Fetal bovine serum
HCl	Hydrochloric acid
O/W	Oil in water
OA-MNP	Oleic acid coated Fe_3O_4 nanoparticle
PLGA	Poly(dl-lactic-co-glycolic acid)
PLGA-MNP	PLGA coated magnetic nanoparticle
PVA	Poly (vinyl alcohol)
M-H	Magnetization versus applied magnetic field
MNP	Fe_3O_4 nanoparticle
NCI	National Cancer Institute
DMSO	Dimethyl sulfoxide
RT	Room temperature
TEA	Triethylamine
XTT	Sodium(2,3-bis(2-methoxy-4-nitro-5-sulphophenyl)-2H-tetrazolium-5-carboxanilide proliferation assay

CHAPTER 1

INTRODUCTION

1.1 Cancer

Cancer is a complex family of diseases identified with unrestrained growth and spread of abnormal cells. It is resulted from multiple changes in gene expression. The mechanisms altering gene expression may take place by gene mutation, translocation, amplification, deletion, loss of heterozygosity and also abnormal gene transcription or translation. The overall result is a dysregulated balance of cell replication and cell death which leads to growth of a tumor cell population (Ruddon, 2007, pp. 4, 7). If the increase in cell numbers is bounded locally then it is described as benign, on the other hand if this uncontrolled cell growth is accompanied by invasion surrounding tissues or spread to distant sites (metastasis) then it is called as malignant (Pellengaris & Khan, 2006, pp. 7, 8). Benign tumors are almost never life threatening.

Some cancers such as leukemia do not form tumors. Generally, cancers are identified according to the organ or type of cell in which they initiate. For instance, cancer which begins in the colon is called colon cancer and breast cancer which has metastasized to the liver is named as breast cancer, not liver cancer (American Cancer Society [ACS], 2012). Types of cancer differ in their age of onset, rate of growth, state of cellular differentiation, metastatic potential, diagnostic detectability, response to treatment and prognosis (Ruddon, 2007, p.7).

Causes of cancer involve both external agents (infectious organisms, tobacco, radiation, and chemicals) and internal agents (hormones, inherited mutations, immune conditions, and mutations which occur from metabolism). These may act together or in sequence to start or contribute to the development of cancer (ACS, 2012). Cancers of the lung, stomach, liver, colon, and breast are the reasons of most cancer deaths, and the frequency of them can differ in sexes (Tuncer, 2010, p. 21). In Turkey, cancer is the second highest cause of death after cardiovascular diseases and the most commonly observed one in males is lung cancer while it is breast cancer in females (Tuncer, 2010, pp. 415, 416).

1.2 Breast Cancer

Breast cancer occurs in tissues of the breast, usually the ducts and lobules. It is observed predominantly in women but it may also occur in men (National Cancer Institute [NCI], 2011). Worldwide, the most common cancer in women is breast cancer and more than 1 million women are diagnosed with it every year. It makes up 23 % of all cancers in women (Coley, 2008).

In addition to being female, risk factors for breast cancer include age factors (increasing age), familial factors (family history of one or more first degree relatives with breast cancer), life and reproductive factors (physical inactivity, alcohol consumption, long menstrual history, never having children and having one's first child after age 30). Moreover, high-dose radiation given to the chest for cancer treatment increases the risk of breast cancer (Washbrook, 2006; ACS, 2012).

Generally, a woman is regarded as being at high risk for breast cancer when she carries a mutation in one of two breast cancer susceptibility genes, *BRCA1* or *BRCA2* (Narod, 2011). The protein product of *BRCA1* has role in DNA repair, transcription, regulation of cell cycle, and protein ubiquitination. Most of the mutations here include shortening of the gene product with resultant loss of function. *BRCA2* codes for a DNA repair protein and similar to *BRCA1*, a mutation in both alleles will cause the loss of a functional DNA repair protein and development of breast and ovarian cancer. In addition, men are at an increased risk for breast cancer when they have a germline *BRCA2* mutation (Tucker & Rizk, 2011).

The main treatments for breast cancer are surgery (removal of the breast or tumor with clear margins), chemotherapy before or after surgery, radiotherapy and also hormone therapy (tamoxifen, aromatase inhibitors). Besides patient preference, tumor size, extent of spread and other characteristics are considered for the selection of treatment type (ACS, 2012).

1.3 Chemotherapy

In chemotherapy anti-cancer drugs are used to cause damage to cancer cells. These drugs can act by stopping cancer cells from growing or multiplying. Once the cancer had spread, surgery and radiotherapy lose their effectiveness. In this case, the systemic delivery of chemotherapy provides that all disease sites receive the anti-cancer treatment. Although, this is an advantage over surgery and radiotherapy, chemotherapy also shows toxicity on healthy cells. Anti-cancer drugs generally cause damage to deoxyribonucleic acid (DNA) or prevent chromosomal replication resulting in programmed cell death (apoptosis) (Bhosle & Hall, 2009).

Chemotherapy drugs are classified according to their mechanism of action (Praetorius & Mandal, 2007; Güç, 2008).

Alkylating Agents: Alkylating agents cause abnormal base pairing or DNA strand breaks by cross-linking guanine nucleobases which leads to stunt tumor growth. Cisplatin and melphalan belong to this group.

Anthracycline Agents: Anthracycline agents function by forming complex with DNA through intercalation between two adjacent nucleotide bases. Thus, they prevent the complex from separating, and interfering with cell replication. They inhibit DNA synthesis and function. Doxorubicin, daunorubicin, idarubicin, and epirubicin belong to this group.

Antimetabolites: These agents are cell cycle specific and act as purines or pyrimidines. They are involved into bulding blocks of DNA or RNA in order to prevent cell divisions of the dividing tumor cells. 6-mercaptopurine and 5-fluorouracil belong to this group.

Plant Alkaloids: These are antitumor agents obtained from plants. They inhibit cell division by preventing microtubules from being synthesized. Vincristine and paclitaxel are typical examples of this group.

Immunotherapeutic Agents: In anti-cancer therapy, these agents may act by decreasing suppressor mechanisms and by stimulating the antitumor response. Thus, they make tumor cells more vulnerable to immunologic defenses. For example, monoclonal antibodies attach to the tumor cells and provoke immune system reaction. In addition to monoclonal antibodies, cytokines or vaccines can be used as immunotherapeutic agents.

1.3.1 Role of Doxorubicin in Cancer Treatment

Doxorubicin (DOX) is an anticancer drug and it is a member of the anthracycline ring antibiotics (Bisht & Maitra, 2009). For treatment of haematological and solid tumors, application of anthracyclines as monotherapy or in combination with other anticancer drugs is a widely used method. On the other hand, they are associated with dose-dependent cardiotoxicity which limits the cumulative dose that can be given (Leonard, Williams, Tulpule, Levine, & Oliveros, 2009).

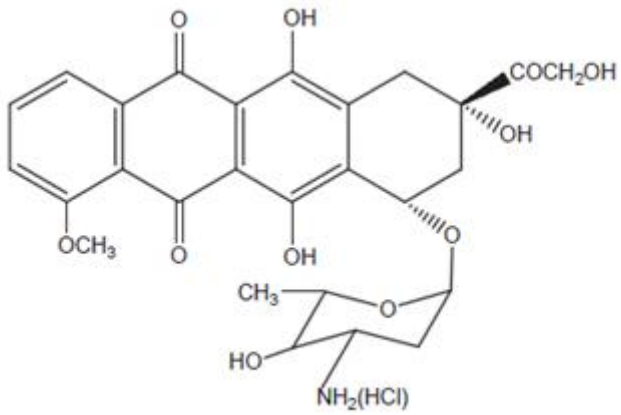

Figure 1.1 Chemical structure of doxorubicin or doxorubicin hydrochloride (Zeng et al., 2005)

Figure 1.1 indicates the structure of doxorubicin. The anthracycline ring is lipophilic and the saturated end of the ring system have many hydroxyl groups near by the amino sugar producing a hydrophilic center. DOX is commonly used in the treatment of a various types of cancers such as lymphoma, acute leukemia, soft-tissue sarcoma, breast, ovarian, and lung cancer. Nucleotide base intercalation and membrane lipid binding activities of DOX lead to cytotoxic effects on cancer cells and various organs. In fact, intercalation inhibits nucleotide replication interfering with the action of DNA and RNA polymerases. Moreover, it causes formation of DNA cleavable complexes by interacting with topoisomerase II. It is generally administered intravenously with a maximum dose of 60-90 mg/m^2 at 21-day intervals (www.accessdata.fda.gov/drugsatfda_docs/label/2003/050467s068lbl.pdf). The commercial form of DOX is usually a water soluble hydrochloride salt (Tewes et al., 2007).

1.4 Drawbacks of Conventional Cancer Treatment

Radiotherapy has a very devastating side effect on the immune system and dividing cells leading to nausea, vomiting, diarrhea and anemia. Surgery can be remedial for early stages of some cancers, with only limited associated morbidity and very low fatality. On the other hand, most cancers could be detected after metastasis, while surgically unreachable cancers such as the ones of intracranial origin cause high mortality and morbidity. Besides, chemotherapy has the disadvantage of high toxicity to the normal tissues due to poor differentiation between normal and cancer cells. In order to deal with these side effects, novel therapeutic options have to be developed. Nanotechnology, especially nanoparticulate drug delivery systems, has potential to overcome these drawbacks of current cancer treatment (Zhang & Chatterjee, 2006).

1.5 Nano Drug Delivery Systems

Nanotechnology, as described by the National Nanotechnology Iniative, is the study and use of structures approximately in the size range of 1 to 100 nm (Mishra, Patel, & Tiwari, 2010). Nanocarriers can bring about several improvements in cancer therapy (Table 1.1). For example, they can stabilize lipophilic drugs in circulation or increase the circulatory duration of drugs by controlled release. Therefore, the toxicity related to the initial high concentrations in periodic doses can be overcome (Zhang & Chatterjee, 2006).

Table 1.1 Objectives and qualifications of targeted nanoscale drug delivery systems*

1. Increase drug concentration in the tumor through:
(a) passive targeting
(b) active targeting
2. Decrease drug concentration in normal tissue
3. Improve pharmacokinetics and pharmacodynamics profiles
4. Improve the solubility of drug to allow intravenous administration
5. Release a minimum of drug during transit
6. Release a maximum of drug at the targeted site
7. Increase drug stability to reduce drug degradation
8. Improve internalization and intracellular delivery
9. Biocompatible and biodegradable

(*Adapted from Danhier, F., Feron, O., & Préat, V. (2010). To exploit the tumor microenvironment: Passive and active tumor targeting of nanocarriers for anti-cancer drug delivery. *Journal of Controlled Release : Official Journal of the Controlled Release Society*, *148*(2), 135-46. Elsevier B.V. doi:10.1016/j.jconrel.2010.08.027)

In Figure 1.2, different types of nanoscale drug delivery systems are shown. Firstly, nanoparticles are solid and spherical compounds. They can be classified into nanospheres and nanocapsules. Nanocapsules are vesicular systems in which drugs are surrounded by a membrane while nanospheres are matrix systems with drugs dispersed throughout (Mishra et al., 2010). Moreover, polymeric micelles are amphiphilic block copolymers generating a nanosized core/shell composition in aqueous solution. The hydrophobic core part act as a place for hydrophobic drugs while hydrophilic shell part stabilizes the hydrophobic core rendering the polymer to be water soluble (Cho, Wang, Nie, Chen, & Shin, 2008). Thirdly, liposomes are spherical self-closed structures consist of lipid bilayers with an aqueous phase inside. Both

hydrophilic and hydrophobic drugs can be entrapped into liposomes (J. H. Park et al., 2008). Another one is highly branched regular three-dimensional macromolecules called as dendrimers (Balogh, 2007). Lastly, polymer–drug conjugates are polymeric macromolecules formed by a polymer backbone on which drugs are conjugated by linker regions (Danhier, Feron, & Préat, 2010).

Nanoparticles are more appropriate for intravenous administration than larger microparticles since they do not form aggregates which is the potential cause of embolism. Moreover, they can pass through the smallest capillaries with 5-6 μm diameter (Hans & Lowman, 2002). The tumor targeting can be achieved basically by active and passive targeting.

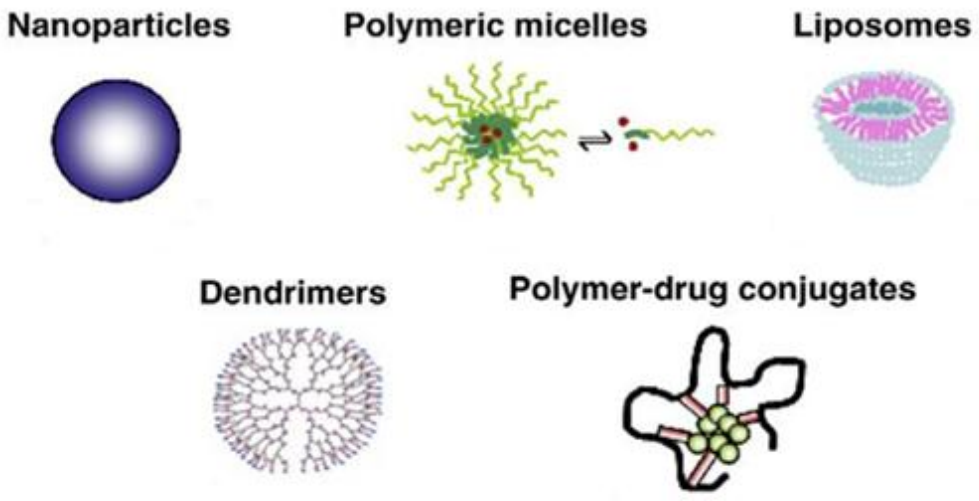

Figure 1.2 Types of nanocarriers (Danhier et al., 2010)

1.5.1 Passive Targeting

Passive targeting utilize the permeability of tumor tissue (Figure 1.3) (Sinha, Kim, Nie, & Shin, 2006). For example, targeting of solid tumor tissue can be achieved through passive mechanism called enhanced permeation and retention (EPR). EPR depends on the fact that tumor cells stimulate production of new blood vessels to grow rapidly. These new blood vessels are poorly organized and have leaky fenestrations. Therefore, small macromolecules and nanoparticles can extravasate out of vasculature, into the tumor tissue. Moreover, there is a poor clearance of these agents due to the inefficient lymphatic drainage. Thus, selective accumulation of these agents is achieved (Veiseh, Gunn, & Zhang, 2010).

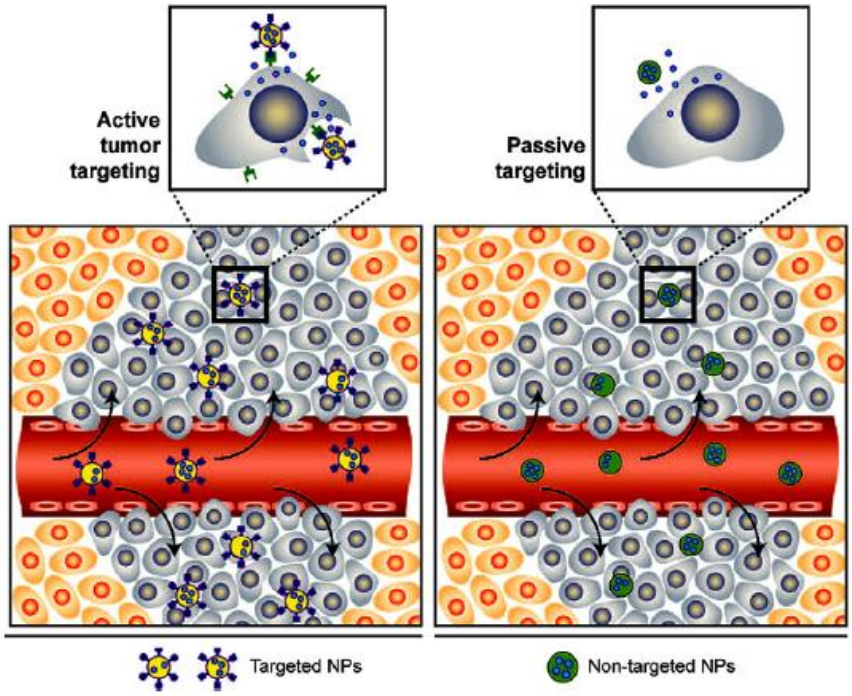

Figure 1.3 Active and passive targeting of nanocarriers (Mahmoudi, Sant, Wang, Laurent, & Sen, 2011)

1.5.2 Active Targeting

Active targeting depends on the over or exclusive expression of different epitopes or receptors in tumoral cells, and on specific physical characteristics. Therefore, vectors sensitive to physical stimuli such as temperature, pH, or magnetism have been developed and conjugated to drugs (Figure 1.3). Another way of active targeting may be with over-expressed species such as low molecular folic acid, thiamine, sugars, peptides (RGD, LHRD) and proteins (Arruebo, Fernández-pacheco, Ibarra, & Santamaría, 2007).

1.6 Magnetic Nanoparticles

Among all types of nanoparticles being explored for biomedical use, magnetic nanoparticles with superparamagnetic characteristics have gained significant attention (Veiseh et al., 2010).

These nanoparticles have been investigated for various biomedical applications such as magnetic resonance imaging contrast enhancement, cancer treatment by hyperthermia, cell separation, magnetofection and targeted drug delivery (Jain et al., 2008).

A potential advantage of using magnetic nanoparticles is the utilization of localized magnetic field gradients for attracting the particles to a chosen site and holding them there until the therapy is complete (Figure 1.4) (Berry & Curtis, 2003).

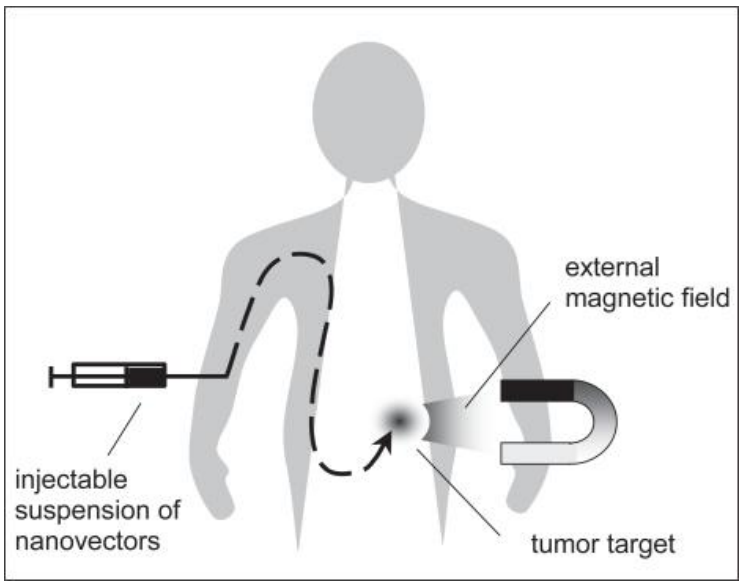

Figure 1.4 Principle of magnetic drug targeting (Laurence Douziech-Eyrolles et al., 2007)

The notion of utilizing magnetic micro-and nano particles for drug delivery was suggested in the late 1970s (McBain, Yiu, & Dobson, 2008) and they have been searched as the next generation of targeted drug delivery for more than thirty years (Chomoucka et al., 2010).

Drug localization with magnetic nanoparticles relies on the competition between forces applied on the particles via the blood portion and magnetic forces resulted from the applied magnetic field (Figure 1.5).

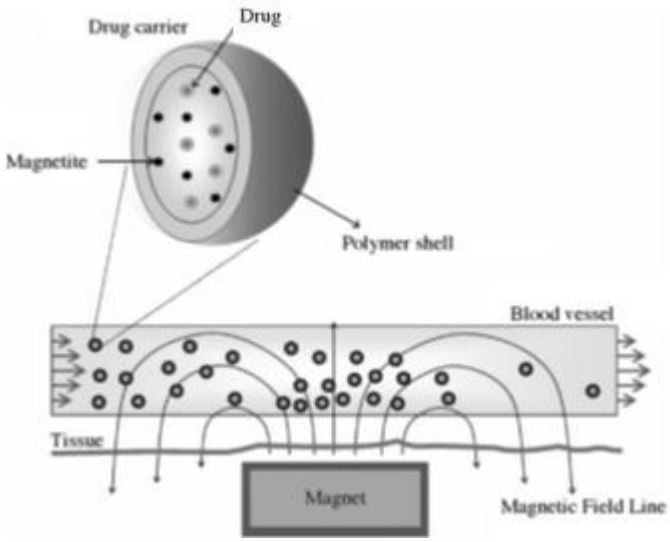

Figure 1.5 Schematic indication of the magnetic drug targeting; magnetic drug carriers are retained at the target region and release the drug (J. Yang, Park, Yoon, Huh, & Haam, 2006).

Generally, the magnetic field gradient is produced by a strong permanent magnet, like Nd-Fe-B which is immobilized outside the body over the target site. The drug loaded carriers, mostly in the form of a biocompatible ferrofluid, are injected into the patient through the circulatory system.

Once the magnetic forces overcome the linear blood flow rates in arteries (10 cm s^{-1}) or capillaries (0.05 cm s^{-1}), the nanoparticles are kept at the target zone by external magnetic fields (Figure 1.5). When the drug loaded carrier is accumulated at the target, the drug can be released either by enzymatic activity or alterations in physiological conditions such as temperature, osmolarity, or pH. Beside this, they can be taken up by the endothelial cells of the target tissue or the tumour cells (Mahmoudi et al., 2011).

1.6.1 Synthesis and Design of a Magnetic Nanoparticle

The basic structure of a biomedical magnetic nanoparticle is comprised of an inorganic nanoparticle core and a biocompatible surface coating that enables stabilization under physiological conditions. In addition, the application of suitable surface chemistry enable the integration of functional ligands (Figure 1.6) (Sun, Lee, & Zhang, 2008).

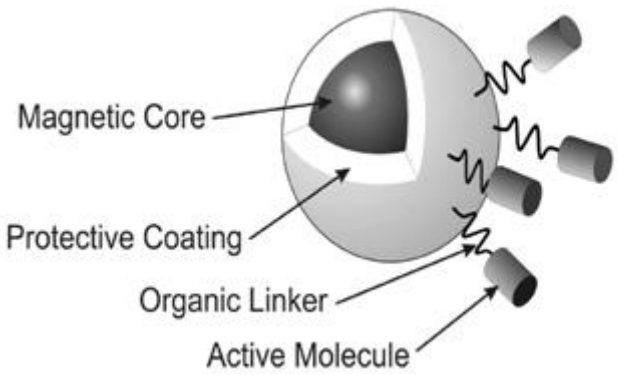

Figure 1.6 A typical design of a magnetic nanoparticle (McBain et al., 2008)

1.6.1.1 Magnetic Core Material

There are many magnetic materials available with a large spectrum of magnetic characteristics. While many of them like cobalt and chromium are highly toxic, iron oxides are relatively safe.

Iron oxides, such as magnetite and maghemite are the most frequently utilized compounds for particle synthesis and they are in use in the clinic as MRI contrast agents (Kumar et al., 2010; McBain et al., 2008).

1.6.1.1.1 Magnetite

Magnetite, Fe_3O_4, has a cubic inverse spinel structure. In this structure, oxygen generates a face centered cubic (fcc) closed packing and Fe cations occupies interstitial tetrahedral sites and octahedral sites (Figure 1.7) (A. K. Gupta & Gupta, 2005). Toxicity of magnetite has been found as quite low (LD_{50} in rats : 400 mg/kg) and well tolerated in the body. In addition, polymer-coated magnetite did not demonstrate any acute or subacute toxicity in experimental animals (Arias, Gallardo, Gómez-Lopera, Plaza, & Delgado, 2001).

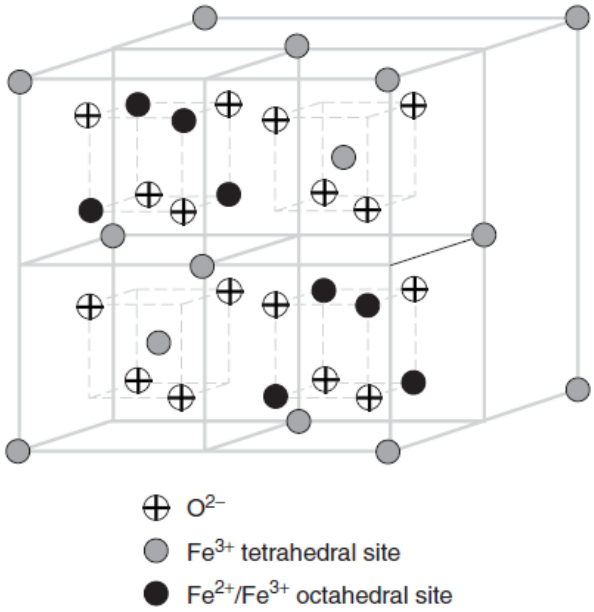

Figure 1.7 Inverse spinel structure of magnetite (Gossuin, Gillis, Hocq, Vuong, & Roch, 2009)

1.6.1.1.2 Synthesis of Fe_3O_4 Nanoparticles

There are many methods have been present to synthesize iron oxide nanoparticles, such as, involving co-precipitation, hydrothermal synthesis, microemulsion and sol–gel.

Among these listed techniques, preparative procedures from precipitation is more applicable, due to its simplicity, efficiency and ability to control the particle size of iron oxides.

1.6.1.1.2.1 Coprecipitation Technique

Synthesis of iron oxides (either Fe_3O_4 or γ-Fe_2O_3) can be through the coprecipitation of Fe^{+2} and Fe^{+3} aqueous salt solutions by addition of a base. Types of salts used, Fe^{+2} and Fe^{+3} ratio, pH and ionic strength of the media can affect the size, shape and composition of nanoparticles. Conventionally, preparation of magnetite is performed by adding a base to an aqueous mixture of Fe^{+2} and Fe^{+3} chloride at a 1:2 molar ratio. The colour of precipitated magnetite is black (A. K. Gupta & Gupta, 2005). The overall chemical reaction of Fe_3O_4 precipitation can be expressed as in Equation 1.1.

$$Fe^{2+} + 2Fe^{3+} + 8OH^- \longrightarrow Fe_3O_4 + 4H_2O \qquad \text{(Eq. 1.1)}$$

A complete precipitation of Fe_3O_4 is expected between pH 9 and 14 due to the thermodynamics of this reaction,while maintaining a molar ratio of Fe^{+3}: Fe^{+2} is 2:1. The reaction should take place under a non-oxidizing oxygen free environment because in the presence of O_2, Fe_3O_4 might also be oxidized to γ-Fe_2O_3.

1.6.1.2 Coating of Magnetic Nanoparticles

Nanoparticles have large surface to volume ratio, therefore, they tend to come together for minimizing their surface energy. This brings about large size aggregates with destroyed magnetic properties. Steric repulsion is generally proposed to prevent agglomeration of nanoparticles. Fe_3O_4 nanoparticles can be coated with surfactants, such as oleic acid ($C_{18}H_{34}O_2$) in order to be sterically stabilized (Andhariya, Chudasama, Mehta, & Upadhyay, 2010). The structure of oleic acid is given in Figure 1.8.

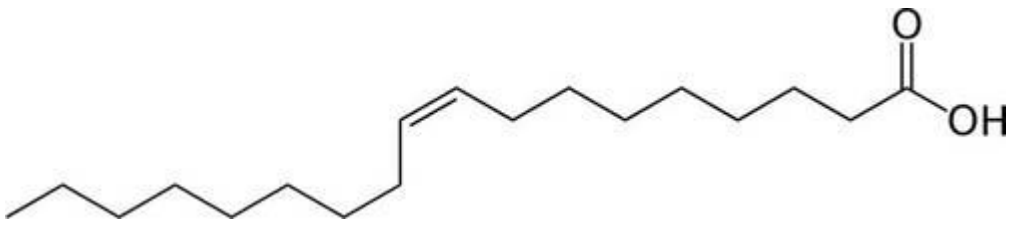

Figure 1.8 Structure of oleic acid

To protect magnetic core materials against corrosion and also to prevent leaching them into the body during in vivo applications, these nanoparticles need to be coated (McBain et al., 2008). Moreover, magnetic nanoparticles by itself are not very proper for drug carrying due to the restrictions on controlling the amount of drug they carry and the rate at which they can release. On the other hand, biodegradable polymers have the ability to release previously absorbed drugs at a rate determined by their degradation (Arias et al., 2001). Therefore, magnetic nanoparticles are usually coated with polymers. Polymeric

materials can be classified into synthetic and natural. Some examples of natural polymers involve gelatin, dextran, chitosan and pullulan. Poly(ethylene-*co*-vinyl acetate), poly(vinylpyrrolidone) (PVP), poly(lactic-*co*-glycolic acid) (PLGA), poly(ethyleneglycol) (PEG) and poly(vinyl alcohol) (PVA) are the typical examples of synthetic polymers (A. K. Gupta & Gupta, 2005).

1.6.1.2.1 Poly(dl-lactic-co-glycolic acid) (PLGA)

Poly(dl-lactic-co-glycolic acid) (PLGA), a copolymer of lactic and glycolic acid, is approved by the Food and Drug Administration (FDA) for drug delivery use (Muthu, 2009). Based on the ratio of lactic acid to glycolic acid, variable types of PLGA can be derived. These copolymers are named according to the monomers ratio used. For example, PLGA 75:25 describes a copolymer whose contents are of 75% lactic acid and 25% glycolic acid (Acharya & Sahoo, 2011).

PLGA is widely used in preparation of nanoparticles for biomedical applications due to their excellent biocompatibility, biodegradability and mechanical strength. Biodegradation of PLGA results in minimal systemic toxicity because the degradation products, lactic and glycolic acids are effectively processed by the body. In fact, lactic acid and glycolic acid participate into the Krebs cycle. Then they are metabolized and eliminated from the body as carbon dioxide and water. Besides, glycolic acid can be excreted unaltered in the kidney (Muthu, 2009).

The molar ratio of the lactic and glycolic acids in the polymer chain, molecular weight of the polymer, the degree of crystallinity and the glass transition temperature of the polymer determines its biodegredation rate. For instance, hydrolyzation of PLGA polymers containing 50:50 ratio of lactic acid and glycolic acids is much faster than those having higher proportion of either of the two monomers. Structure of PLGA is given in Figure 1.9, where m and n indicate the number of units of lactic acid and glycolic acid, respectively.

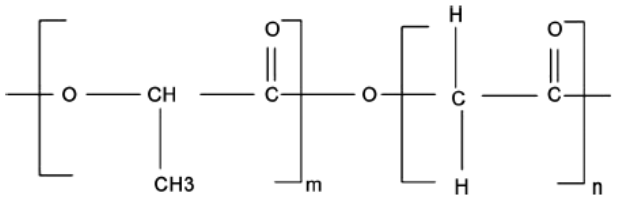

Figure 1.9 Structural formula of PLGA (Muthu, 2009)

There are many techniques present for the preparation of PLGA particles. The oil in water (O/W) emulsion evaporation method, the spontaneous emulsification-solvent diffusion method, the nanoprecipitation method and the spraying method are the examples of techniques used in preparing PLGA nanoparticles of various size.

1.6.1.2.1.1 Oil in Water Emulsion Evaporation Method

Emulsification is one of the most applied techniques to prepare PLGA nanoparticles. Usually, hydrophobic PLGA is dissolved in an organic solvent and the organic phase is emulsified with an aqueous phase to make an O/W single emulsion. Removal of the organic solvent ends up with solid particle (Tewes et al., 2007).

One of the most widely used emulsifier to stabilize the emulsion is poly (vinyl alcohol) (PVA) (Acharya & Sahoo, 2011). The structure of PVA is given in Figure 1.10. The hydrophilic group is polyhydric alcohol and the lipophilic group is fatty acid. The lipophilic part of the PVA aligns with the solvent droplets while the hydrophilic part extends into the aqueous solution generating an electrostatic barrier against droplet coalescence.

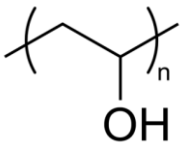

Figure 1.10 Chemical structure of PVA

1.6.2 Magnetic Properties of Materials

The magnetic properties of the materials are originated from the motions of electrons of atoms. These are spin motion and orbital motion, each of which has a magnetic moment related to itself. Spin moment results from spinning of an electron around an axis of itself. The other magnetic moment comes from the spinning of electron along orbit around the nucleus of atom. Net magnetic moment is the sum of these two moments (Eken, 2008). Filled electron subshells in an atom do not affect the magnetic momentum of the atom due to the fact that they have a net angular momentum of zero (Turton, 2000, p. 215). Diamagnetism, paramagnetism and ferromagnetism are the main types of magnetism. Ferromagnetism can be classified into antiferromagnetism and ferrimagnetism (Eken, 2008).

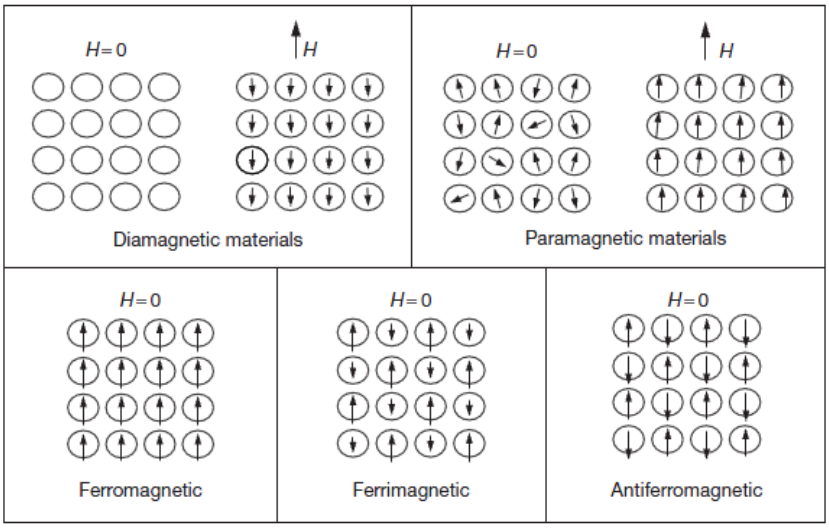

Figure 1.11 Schematic explanation of magnetic dipoles' arrangements for different types of materials in the absence or presence of an external magnetic field (H) (Epherre et al., 2011)

All materials exhibit at least one of these types and they are classified depending on how they behave upon exposure and removal of the magnetic field (Figure 1.11).

Types of magnetism are explained as follows:

- **Diamagnetism:** Presence of magnetic field affects the orbital motion of the electrons in atoms of diamagnetic materials in a manner that the atom produces a magnetic field which is antiparallel to the external field (Figure 1.12) These materials have weak induced dipoles in the presence of a field (Figure 1.11).

- **Paramagnetism:** When there is no external magnetic field present, the spins of electrons of paramagnetic materials are randomly oriented (Figure 1.11). Thus, the magnetic moment in any given direction averages to zero. In an external field, these randomly oriented spins are aligned parallel to the field (Figure 1.12) (Turton, 2000, p. 217, 218).

- **Ferromagnetism:** Ferromagnetic materials retain their magnetization even in the absence of a magnetic field. They have aligned adjacent magnetic dipoles (Figure 1.11). In a ferrimagnetic material there are always weaker magnetic dipoles in the absence of an external magnetic field and their adjacent magnetic dipoles are antiparallel but unequal magnitude.

For an antiferromagnetic material, the adjacent dipoles are antiparallel in the absence of an external field and cancel each other (Figure 1.11) (Epherre et al., 2011; Turton, 2000, p. 227).

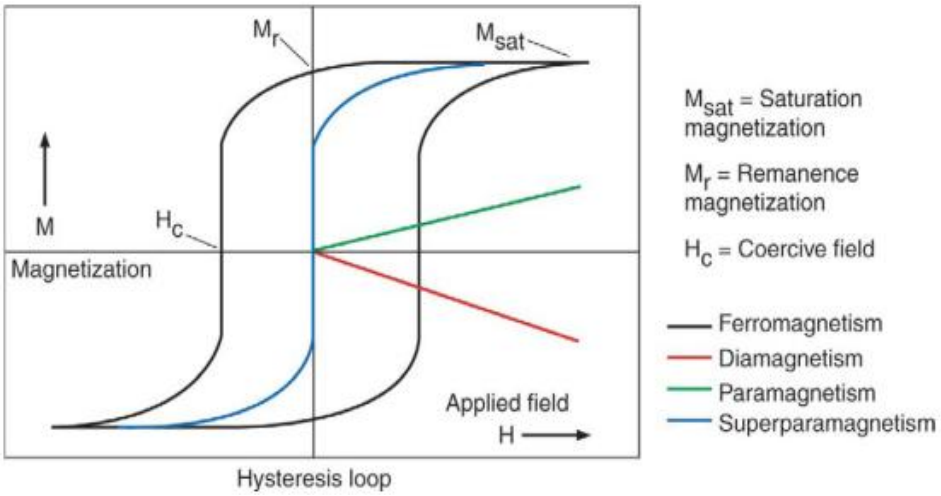

Figure 1.12 Magnetization versus applied magnetic field (M-H) curve for different types of magnetic behaviors (Arruebo et al., 2007)

Different types of magnetic behaviors are indicated in Figure 1.12, where M is the magnetization, H is the strength of magnetic field, Ms is the saturation magnetization (the maximum value of M), Hc is the coercive field (the external field required to reduce the magnetization back to zero) and Mr is the remanent magnetization (the residual magnetization at zero applied field strength) (Epherre et al., 2011). As shown in Figure 1.12, ferromagnetic materials have hysteresis loop with Mr and Hc. In addition, they have higher Ms compared to paramagnetic materials.

1.6.2.1 Superparamagnetism

When the size of the particles are reduced to a certain value, their magnetic characteristics change since the multidomains become single domain state (Can, 2005).

Superparamagnetism is related to the thermal effects in a material. Superparamagnetic particles have strong thermal fluctuations which spontaneously demagnetize a formerly saturated particle. As a result, these particles have zero coercivity and they do not show any hysteresis (Figure 1.12) (Chomoucka et al., 2010). These particles like paramagnetic materials in several aspects such as they do not have hysteresis and remenance at certain temperatures, on the other hand, they have high magnetic saturation values like ferromagnetic materials (Can, 2005).

Superparamagnetic nanosystems are prefered for drug delivery applications. This is due to the fact that nanocarriers with superparamagnetic character are capable of being magnetized when they are exposed to a magnetic field but they do not remain magnetization once the field is turned off (Chomoucka et al., 2010). Thus, agglomeration of nanoparticles that may lead to embolization of capillary vessels is avoided (Arruebo et al., 2007).

1.7 Goals of the Study

The objective of this study was the synthesis of PLGA coated magnetic nanoparticles and load them with anti-cancer drug doxorubicin. The main steps of this study can be summarized as follows:

- To synthesize Fe_3O_4 magnetic nanoparticles (MNP) and coat the surface of MNP with oleic acid (OA-MNP)

- To encapsulate OA-MNP into poly(dl-lactic-co-glycolic acid) (PLGA)

- To characterize prepared nanoparticles according to their physical, chemical and magnetic properties

- To load doxorubicin into PLGA-MNP

- To investigate the cytotoxicity of prepared nanoparticles *in vitro.*

CHAPTER 2

MATERIALS AND METHODS

2.1 MATERIALS

2.1.1 Materials for Magnetic Nanoparticle Synthesis, Polymer Coating, and Drug Loading Studies

Iron(II) chloride tetrahydrate ($FeCl_2.4H_2O$) and iron(III) chloride hexahydrate ($FeCl_3.6H_2O$) used in synthesis of magnetite nanoparticles were purchased from Sigma-Aldrich. Ammonium hydroxide (NH_4OH, %32 of ammonia) was obtained from Merck. Oleic acid was purchased from AppliChem. N_2 gas was obtained from ASYAGAZ. Poly(dl-lactide-co-glycolide) (PLGA, 75:25) (MW: 66.000-107.000), polyvinyl alcohol (PVA) (MW: 30.000-70.000), and dichloromethane (DCM) which were used in polymer coating and drug loading studies were purchased from Sigma-Aldrich. HCl (% 37, v/v) was obtained from Merck. Dimethyl sulfoxide (DMSO) and triethylamine (TEA) were purchased from Sigma-Aldrich. Doxorubicin.HCl (579.98 g/mol) was kindly donated by Prof. Dr. Fikret Arpacı and Prof. Dr. Ali Uğur Ural from Gülhane Military Medical School Hospital (Ankara).

2.1.2 Materials for Cell Culture Studies

MCF-7 monolayer type human epithelial breast adenocarcinoma cell line was donated by ŞAP Institute, Ankara-Turkey.

RPMI 1640 medium ((1x), 2.0g/l $NaHCO_3$, stable glutamine), fetal bovine serum (FBS) were purchased from Biochrom Ag. (Germany).

XTT cell proliferation kit, 0.5% tryphan blue solution, gentamycin sulphate and 0.25% Trypsin-EDTA solution were obtained from Biological Industries, Kibbutz Beit Haemek (Israel).

Dimethylsulfoxide (cell culture grade) was purchased from AppliChem (Germany).

2.2 METHODS

2.2.1 Synthesis of Magnetite Nanoparticles

In this study, magnetite nanoparticles were synthesized by using coprecipitation technique with minor changes (Okassa et al., 2007). For the experiment, five-necked round bottom flask was used. Briefly, $FeCl_2.4H_2O$ and $FeCl_3.6H_2O$ with a molar ratio of Fe(II) /Fe(III) = 1:2 were vigorously mixed in 150 ml deionized water (dH_2O). After stirring for 1 hour, 25 ml NH_4OH (%32, v/v) was added dropwise to the mixture under continuous mechanical stirring at 90°C. In the presence of O_2, magnetite could turn into maghemite. Therefore, N_2 gas was bubbled into the solution to obtain an inert atmosphere during the reaction. Then magnetic decantation was performed and black precipitates of Fe_3O_4 was washed several times with dH_2O until the medium pH decreased to 9.0. At the end of washing step, mixture of nanoparticles was equally divided into two parts. One part was kept as naked Fe_3O_4 (MNP) and second part was kept for oleic acid coating process.

2.2.2 Oleic Acid Coating on Magnetite Nanoparticles

After synthesis of MNP, they were coated with oleic acid (Okassa et al., 2007). Briefly, 8 ml oleic acid was added to second part of the mixture of precipitated nanoparticles and stirred at room temperature for 1 hour. Finally, the oleic acid treated MNPs (OA-MNP) were washed 3 times with 20 ml acetone to get rid of excess oleic acid.

2.2.3 Preparation of Magnetic Polymeric Nanoparticles

In this study, O/W emulsion method was used to prepare polymer coated magnetic nanoparticles. Briefly, certain amount of OA-MNP was dispersed in 2 ml dichloromethane (DCM) through ultrasonication for 5 min in an ice bath. Then this dispersion was mixed with an organic solution of the polymer (100 mg PLGA in 2 ml DCM) by vortex. 4 ml of an aqueous PVA solution (3% w/v) was added to this mixture and then it was emulsified by ultrasonication for 30 sec (90% amplitude). The obtained emulsion was diluted in 50 ml aqueous PVA solution (0.3% w/v). The organic solvent was evaporated overnight under mechanical stirring with a rotation rate of 500 rpm. Through volatilization of the DCM, PLGA hardened and trapped the magnetite within the entangled PLGA chains (Figure 2.1). For optimization studies dried OA-MNPs were added in variable iron oxide/polymer ratio of 1:1, 1:2; 1:4 and 1:8 w/w.

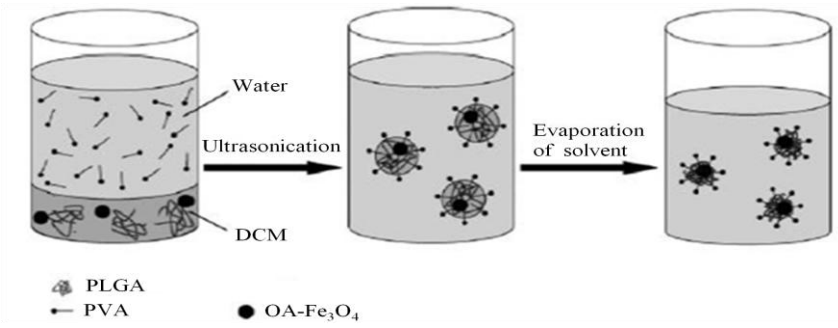

Figure 2.1 Schematic representation of polymer coating process

After solvent removal, the PLGA-MNPs were obtained by centrifugation at 15000 rpm for 50 min at 4˚C. The particles were washed twice with dH_2O and redispersed in 50% aqueous solution of HCl (%32, v/v) to remove unloaded Fe_3O_4 nanoparticles.

Then, the nanoparticles remaining in the pellet were washed with dH_2O twice and stored at 4 ˚C. Preparation of magnetite free PLGA nanoparticles (PLGA-NP) was the same as described above with the exception that no OA-MNP was added to the organic phase.

2.2.3.1 Magnetic Content and Entrapment Efficiency Determination

To find out the amount of Fe_3O_4 content in polymer coated MNPs, the PLGA-MNPs were collected by centrifugation at 15000 rpm for 50 min at 4 ˚C after solvent evaporation process. Then the pellet was treated with 6N HCl to get rid of unloaded OA-MNPs. After HCl treatment, particles were washed with dH_2O and polymer was dissolved by DMSO. Then the particles were washed with dH_2O again and treated with 6N HCl to dissolve iron content in polymeric nanoparticles. The iron concentration in both acidic solutions were determined by AAS measurements. The amount of the loaded magnetite was estimated from the amount of iron measured. Magnetic content (% w/w) and entrapment efficiency (%) were calculated by equation 2.1 and 2.2, respectively.

Magnetic content (% w/w) = (amount of OA-MNP in PLGA-MNP/amount of PLGA-MNP) x 100 (Eq. 2.1)

Entrapment efficiency (%) = (amount of OA-MNP in PLGA-MNP/amount of OA-MNP initially used) x 100 (Eq.2.2)

2.2.4 Conversion of DOX-HCl into Water-Insoluble Doxorubicin

Doxorubicin hydrochloride (DOX-HCl) was used in this study. HCl salt form of it is soluble in water. On the contrary, its base form is almost not dissolved in water but soluble in organic solvents. Thus, DOX-HCl can be used as a hydrophilic drug form while its base type can be used as a lipophilic drug form. To be encapsulated by O/W technique, doxorubicin should be used in a more lipophilic molecular form. Therefore, in this study DOX-HCl was treated with trietylamine (TEA) before loading drug into the polymeric nanoparticles. HCl combines with TEA to form the salt triethylamine hydrochloride. TEA treatment induces the solubilization of drug in dichloromethane. Briefly, predetermined amount of DOX•HCl was stirred with 5 molar equivalents of TEA in DCM for 24 hours.

2.2.5 Preparation of Doxorubicin Loaded Magnetic Polymeric Nanoparticles

The procedure followed to prepare doxorubicin loaded magnetic polymeric nanoparticles was the same O/W emulsion-evaporation method which is explained in section 2.2.3. Different from that, in this part 1 ml of DOX dissolved in DCM (2 mg/ml) was added together with OA-MNP into the organic phase (Figure 2.2). In addition, evaporation process was performed in

dark and after the purification step, unloaded free drug was separated from the MNPs by a magnet.

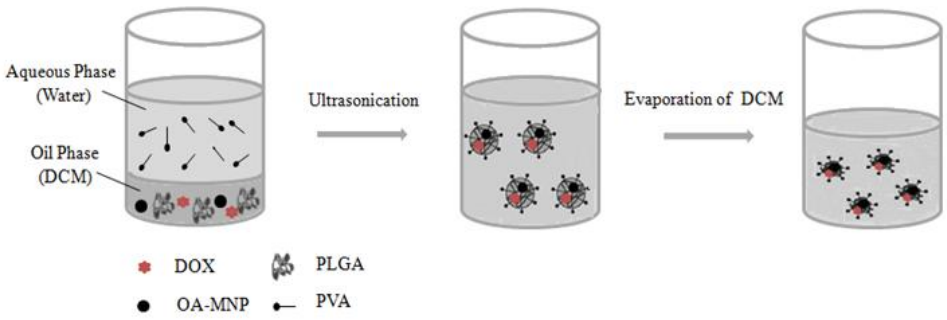

Figure 2.2 Schematic representation of drug loading process

In addition, as a preliminary drug extraction study, freeze dried DOX-PLGA-MNPs (2 mg) were dispersed in DMSO (2 ml) and samples were vortexed in every half hour. After 3 hours, centrifugation was performed at 12000 rpm for 30 minutes and the absorbance of supernatant was measured by UV spectrophotometer (Shimadzu, UV-1208) at λ = 480 nm for DOX. Empty nanoparticles were used a blank. Standards were prepared from known concentrations of DOX in DMSO.

2.2.6 Cell Culture Studies

2.2.6.1 Cell Line and Culture Conditions

MCF-7, a human breast carcinoma cell line, was used as parental cell line in this study. It was first isolated in 1970 from the breast tissue of a 69-year old Caucasian woman and retains several characteristics of differentiated mammary epithelium.

MCF-7 cell cultures were propagated as monolayers in 25 or 75 cm^2 polystyrene tissue culture flasks by RPMI 1640 medium which was supplemented with 10 % (v/v) fetal bovine serum (FBS) and 1% (v/v) gentamycin. Cells were grown under well-established conditions in a Heraus incubator, where the temperature was 37 °C with a controlled humidified gas mixture of 5% CO_2 and 95% O_2.

2.2.6.2 Maintenance

MCF-7 cell cultures were checked in regular and routine intervals. The cell morhology and cell density were observed by microscope. The color and the turbidity of the medium were observed macroscopically. Not to allow media becoming acidic and cells being deprived of specific nutrients, media were changed regularly.

2.2.6.3 Passage of Cells

When the cells have reached confluency (80-90 % of the surface area of a flask was covered with cells), then they were subcultured or passaged to preserve healthy growth. For this purpose, cells were harvested by trypsinization under sterile conditions in Bioair Laminar Flow (Euroclone, Pavia, Italy). Old cell culture medium was discarded and cells were washed with 2-3 ml PBS to remove residual serum which will inactivate trypsin. Then 2 ml trypsin-EDTA solution was added to 75 cm^2 flask and cells were incubated at 37 ˚C for 5-10 min in incubator. The detachment of cells were checked at intervals by microscope. After detachment of cells, fresh culture medium containing serum was added to inactivate the trypsin in the cell suspension and required number of cells were transferred to a new flask. For MCF-7 cell line 1/3 passage ratio was found to be optimum.

2.2.6.4 Viable Cell Counting

Calculation of cell number is an important measurement both for setting up experiments with cell lines and investigating cell response to experimental conditions.

For the purpose of cell counting required for cell proliferation assay, cells were trypsinized and homogenized as it was done in cell passage. Appropriate amount of cell suspension was mixed with tryphan blue solution (0.5%) with the ratio of 9:1. The principle of this method depends on the fact that live cells do not take up tryphan blue dye, whereas dead cells do. Therefore, dead cells

are stained into blue while alive ones exclude the dye. Cells in tryphan blue solution were counted by Hemocytometer (Neubauer, Bright-line, Hausser Scientic, USA) with 100X microscope magnification under phase contrast microscopy (Olympus, USA). A hemacytometer consists of 16 large squares each of which has 16 small squares. The volume of one small square is 0.00025 mm^3. The number of cell in 1 mL was determined using the following formula (Equation 2.3):

Cell number/ml= Average count per square x Dilution factor x 4.10^6 (Eq. 2.3)

2.2.6.5 Cell Freezing and Cell Thawing

When MCF-7 cells were not in use, they were freezed. DMSO was used as a cryoprotectant in freezing medium (10 % DMSO + 90 % FBS) in order to prevent formation of ice crystals and fragmenting of membranes. For the purpose of freezing cells, cells were detached and 5 ml medium was added on them. Cell suspension in 15 ml falcon tube was centrifuged at 1000 rpm for 5 min at 4 ^oC. After discarding supernatant, cells were washed with 5 ml PBS and centrifuged again at 1000 rpm for 5 min at 4 ^oC. At the end of washing step, cells were resuspended in freezing medium and taken into cryovials (Greiner). Cells were incubated firstly at 4 °C for 30 min, at -20 °C for 3-4 hours before overnight incubation at -80°C, finally in liquid nitrogen for longer periods (Dönmez, 2010). For the purpose of thawing frozen cells, cells were taken from -80˚C or -196˚C and kept in 37˚C incubator until it thaws completely. The rate of thawing should be rapid because DMSO is toxic to the cells above +4 ^oC.

2.2.6.6 XTT Cell Proliferation Assay

Cell proliferation assay with XTT reagent was used to investigate the effects of prepared nanoparticles on cell proliferation of MCF-7 cell lines. This colorimetric assay depends on the activity of live cells. Basically, mitochondria enzymes reduce tetrazolium salt XTT to orange colored compounds of formazan. The dye produced is water soluble and its concentration depends on the number of active cells. Its intensity can be read at a given wavelength with a spectrophotometer (Biological Industries, 2002).

The XTT assay was performed in 96-well plates (Şen, 2009). The nanoparticles were sterilized with UV irradiation before use (Wuang, Neoh, Kang, Pack, & Leckband, 2007). Briefly, MCF-7 cells at a concentration $1x10^4$ cells/well were seeded on day 1. The wells belonging to medium control (nothing but the complete growth medium) and sample control (blank) were left empty (Figure 2.3). Cells were attached to the surface of the well after 24 h. On day 2, old medium was replaced with 150 µl of fresh medium for all wells, except the wells of 3rd column. 300 µl of highest sample concentration was added into the wells of the 3rd column. The sample was diluted horizontally by taking 150 µl portion of sample solution from the third column and putting into the next column (1/2 serial dilution).

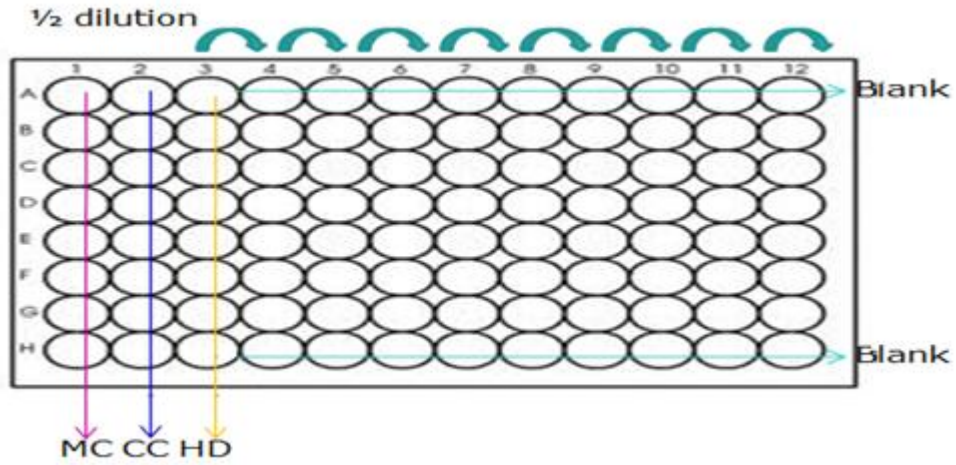

Figure 2.3 Schematic view of XTT assay. MC: Medium control, CC: Cell control, HD: Highest dose and Blank: Wells containing samples but no cells

After 72 h of incubation at 37 °C and 5% CO_2, XTT and activator reagents were applied to each plate and the plates were incubated in dark for 3-4 h. The intensity of color change was measured using ELISA reader (Anthos 2010, England) at 492 nm. The results were stated as percentages relative to the result obtained with the cell control. All the experiments were applied in triplicates.

2.2.6.6.1 Statistical Analysis

Graphpad Software was used to determine the significant differences between results. Results were subjected to one way ANOVA test. Eperimental values are given as ±SEM. The mean difference was significant at the 0.05 level. All the experiments were done in triplicates.

2.3 CHARACTERIZATION STUDIES

The crystalline phase of magnetic nanoparticles was investigated by X-ray Diffraction Analysis (XRD) using a Rigaku Ultima-IV X-Ray diffractometer. Fourier Transform Infrared (FTIR) spectroscopy is used to obtain information about the structure and purity of the prepared nanoparticles with a Thermo Scientific Nicolet 6700 FT-IR Spectrometer in 4000-400 cm^{-1} spectrum range with KBr pellet method.

Morphology and shape of nanoparticles were observed with Scanning Electron Microscopy (SEM) examinations by FEI Quanta 200 FEG, between 500 V and 30 kV. Size and morphology of prepared nanoparticles were also investigated with Transmission Electron Microscope (TEM), Hitachi S-4800. Thermogravimetric measurements were characterized on thermogravimetric analyzer (Perkin Elmer Pyris 1) under nitrogen atmosphere at a heating rate of 10˚C/min from room temperature to 600 ˚C. Magnetic content and entrapment efficiencies of prepared PLGA-MNPs were investigated with Atomic Absorption Spectrophotometer (Shimadzu-6300). Magnetization measurements of samples were performed by Vibration Sample Magnetometer (VSM) (EV/9, ADE Magnetics) with a sensitivity of 10^{-6} emu and a maximum magnetic field of 22 kOe, at both room temperature (23˚C) and body temperature (37˚C).

CHAPTER 3

RESULTS AND DISCUSSION

3.1 Synthesis and Characterization of Iron Oxide Nanoparticles

Magnetic iron oxide nanoparticles were synthesized by chemical coprecipitation technique. Then, they were coated with oleic acid to make them compatible with organic phase containing PLGA in polymer coating process. Prepared nanoparticles were characterized with respect to crystallite structure, composition, size, particle morphology, and magnetic properties by XRD, FTIR, TGA, TEM, and VSM measurements.

3.1.1 X-ray Diffraction Analysis

X-ray Diffraction (XRD) analysis was used to determine the crystalline nature and phase purity of magnetic nanoparticles. XRD pattern of synthesized MNPs is shown in Figure 3.1.

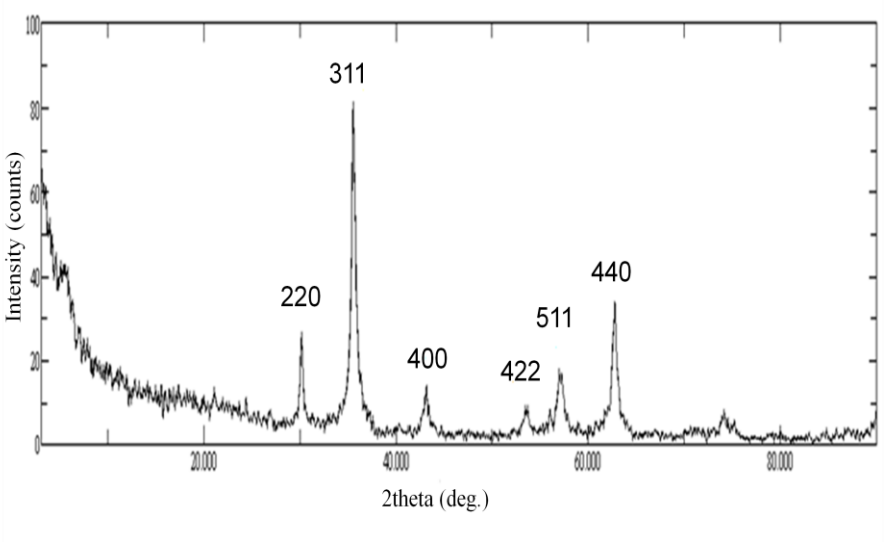

Figure 3.1 XRD pattern of MNP

Briefly, diffraction peaks at (220), (311), (400), (422), (511), and (440) were present in XRD pattern of MNP and they corresponded to characteristic peaks of the Fe_3O_4 crystal with a cubic spinel structure. Experimental *d* spacings calculated from the XRD pattern and standard data from ICDD (The International Centre for Diffraction Data) cards are given in Appendix A.

There are different types of iron oxides with magnetic properties other than magnetite, such as maghemite (γ-Fe_2O_3) and hematite (α-Fe_2O_3) (Gou et al., 2008). It is mentioned that magnetite can be oxidized to maghemite and this can be later turned into hematite at high temperatures. The characteristic diffraction peaks of hematite and maghemite are at (213), (210), (113), and (210), respectively (Liu *et al*., 2006).

As shown in Figure 3.1, there were no peaks which could belong to impurities such as γ-Fe_2O_3 or α-Fe_2O_3. Thus, it can be stated that only Fe_3O_4 was detected in synthesized nanoparticles.

3.1.2 Fourier Transformed Infrared Spectroscopy

Fourier transform infrared spectroscopy (FTIR) measurements were performed for both MNP and OA-MNP. The infrared spectra of MNP and OA-MNP are shown in Figure 3.2. The band at 580 cm^{-1} in FTIR spectrum of MNP belonged to vibrations of the Fe-O bonds of magnetite (Figure 3.2(a)) (Liu et al., 2006). Two bands at 1630 and 3401 cm^{-1} were also observed. These were the characteristic bands of hydroxyl groups which might have covered the surface of MNP in aqueous environment during the coprecipitation process (K. Yang, Peng, Wen, & Li, 2010).

The band of Fe-O bond shifted to 573 cm^{-1} in FTIR spectrum of OA-MNP (Figure 3.2(b)) and five new bands at 1431, 1525, 1708, 2849 and 2918 cm^{-1} were present differently from MNP. Two sharp bands at 2918 cm^{-1} and 2849 cm^{-1} corresponded to the asymmetric CH_2 stretching and the symmetric CH_2 stretching in oleic acid, respectively (Coates & Ed, 2000). Adsorption of oleic acid on iron oxide surface can be confirmed by the bands at 1431 cm^{-1} (V_s: COO^-) and 1525 cm^{-1} (V_{as}: COO^-) which might be attributed to oleate ion immobilized on the iron oxide surface (Okassa et al., 2007).

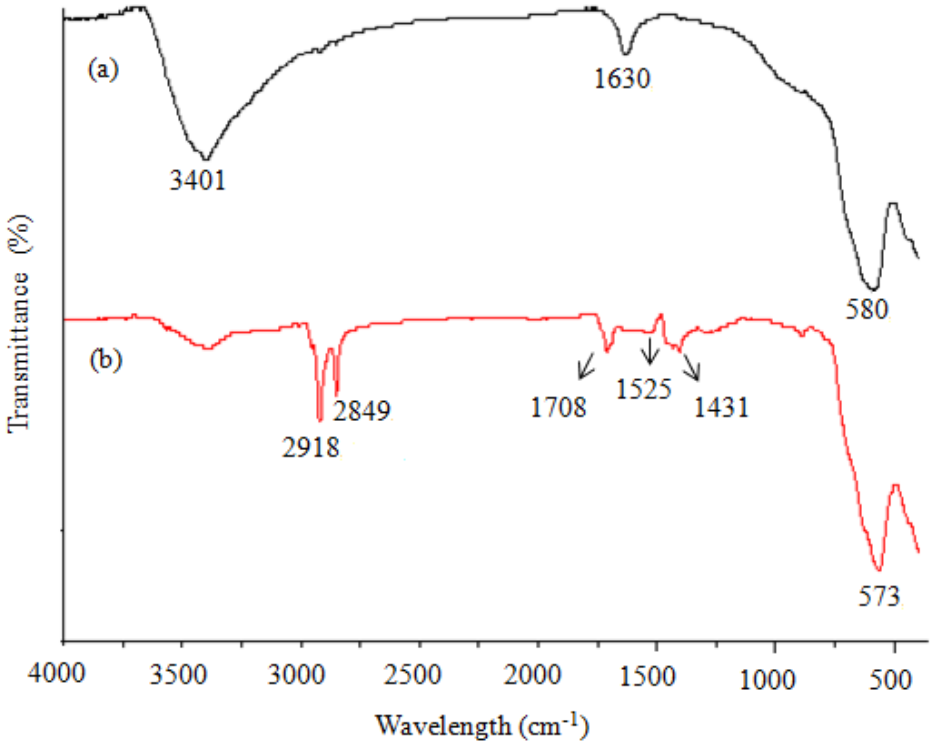

Figure 3.2 FTIR spectra of (a) MNP and (b) OA-MNP

ATR spectrum of pure oleic acid was compared with FTIR spectrum of OA-MNP (Figure 3.3). Zhang *et al* mentioned that C=O stretching band of the carboxyl group which was present at 1710 cm^{-1} in the spectrum of pure oleic acid was absent for oleic acid coated nanoparticles (Zhang, He, & Gu, 2006). In this study, this band was present at 1708 cm^{-1} in the spectrum of OA-MNP (Figure 3.3 (a)). On the other hand, the carboxylate bands indicating the oleic acid adsorption on the surface of iron oxide were also present. As a result, it could be interpreted that both oleic acid molecule and oleate molecules existed on magnetite surface (Liu et al., 2006).

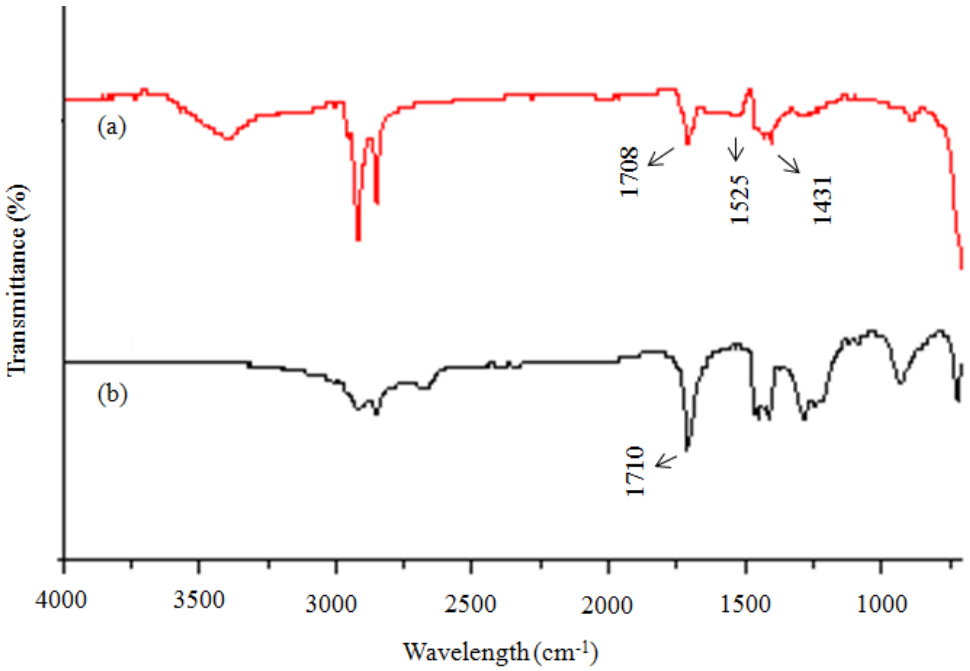

Figure 3.3 FTIR spectrum of (a) OA-MNP and (b) ATR spectrum of pure oleic acid

Zhang *et al* mention that the interaction between the carboxylate head of oleic acid and metal atom could be categorized into four types. These are monodentate, bridging (bidentate), chelating (bidentate) and ionic interactions. Type of interaction can be determined by using the wavenumber separation, λ, between the V_{as} (COO^-) and V_s (COO^-) infrared bands. Here, the λ (1525-1431 = 94) pointed out the chelating bidentate interaction indicated in Figure 3.4 (L. Zhang et al., 2006).

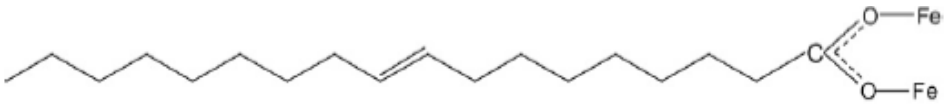

Figure 3.4 Schematic representation of chelating bidentate interaction between the oleic acid and iron oxide nanoparticle (L. Zhang et al., 2006).

3.1.3 Hydrophobicity Test

Hydrophobicity of oleic acid coated nanoparticles were shown via dispersing them in a water/DCM mixture.

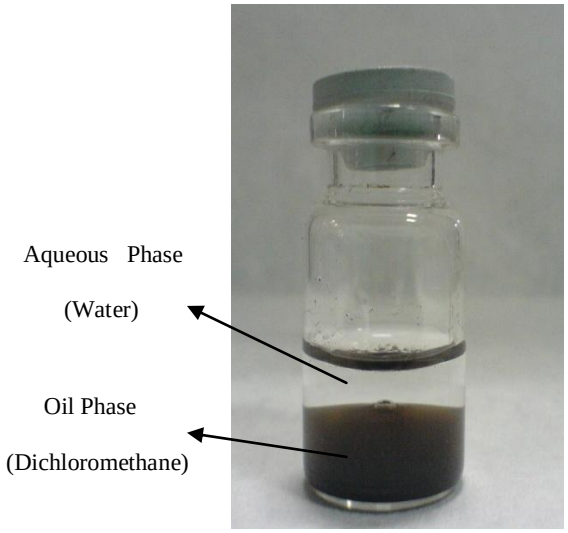

Figure 3.5 Photograph of OA-MNP dispersed in water/DCM mixture

The oil phase of DCM existed below water due to its higher density (Figure 3.5). OA-MNPs partitioned to the oil phase (DCM) due to their hydrophobic nature. Results of both FTIR spectroscopy and hydrophobicity test revealed that hydrophilic magnetite nanoparticles were coated with oleic acid.

3.1.4 Transmission Electron Microscopy

Size and morphology of MNP and OA-MNP were examined by transmission electron microscopy (TEM) (Figure 3.6 and 3.7). As shown in TEM images of MNP (Figure 3.6), nanoparticles were agglomerated and the size of the particles in clusters were between 5 and 30 nm. In fact, magnetic nanoparticles have large surface to volume ratio, thus they have a tendency to aggregate for reducing their surface energy. Steric repulsion is generally utilized to prevent the agglomeration (Andhariya et al., 2010) and in this study oleic acid was used to produce the sterically stabilized Fe_3O_4 nanoparticles.

TEM images of OA-MNP shown in Figure 3.7 indicate that MNPs were dispersed by certain degree after oleic acid coating. Moreover, the particles were spherical in shape with a diameter of 10-15 nm.

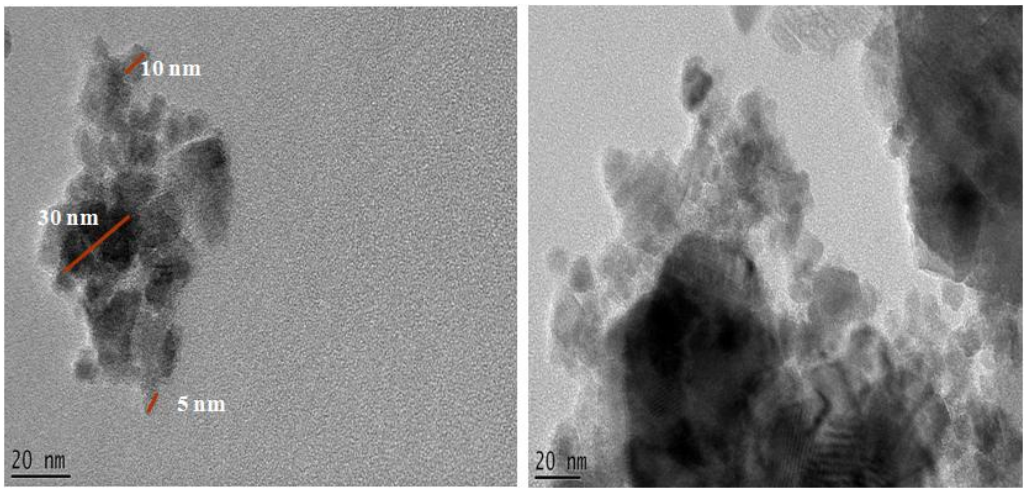

Figure 3.6 TEM images of MNP dispersed in water

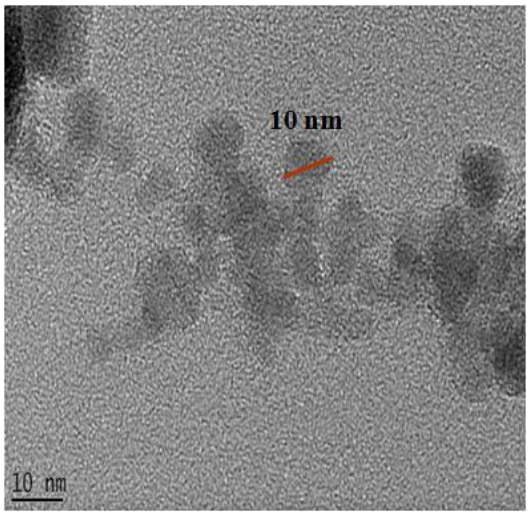

Figure 3.7 TEM image of OA-MNP dispersed in ethanol

3.1.5 Thermogravimetric Analysis

Thermogravimetric analysis (TGA) was performed to determine the weight percentage of oleic acid on the iron oxide surface. Figure 3.8 shows the TGA curves of MNP and OA-MNP. For MNP, the 2 % weight loss could be attributed to evaporation of water.

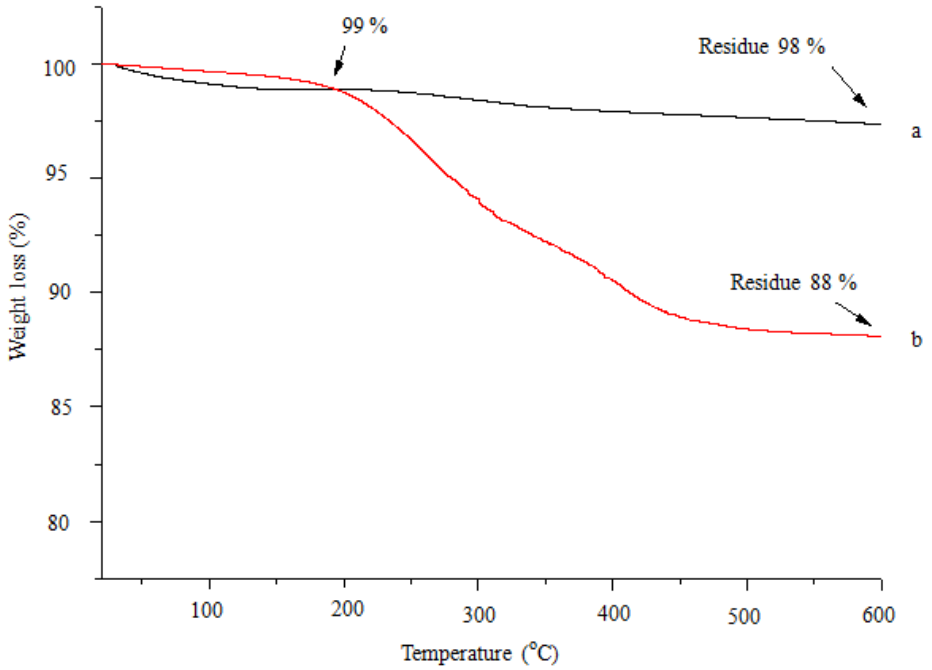

Figure 3.8 TGA curves of (a) MNP and (b) OA-MNP

TGA curve of OA-MNP exhibits two steps of weight loss in the temperature ranges of 20-140 ^{o}C and 140-600 ^{o}C.

The first slight amount of weight loss (1%) could be attributed to evaporation of water (C. E. Astete, Kumar, & Sabliov, 2007). The second weight loss due to the decomposition of surfactant from nanoparticle surface began at 140 ^{o}C and ended below 600 ^{o}C. The TGA residue for MNP at 600 ^{o}C was 98% and it was 88% for OA-MNP. The amount of oleic acid adsorbed on the surface of MNP was estimated as 11 % from TGA results.

3.1.6 Vibration Sample Magnetometer Analysis

Magnetic properties of MNP and OA-MNP at both room (23^{o}C) and body temperatures (37^{o}C) were investigated by using vibration sample magnetometer (VSM) analysis.

The saturation magnetization values (Ms) of bare MNP and OA-MNP at room temperature were 62 emu/g and 53 emu/g, respectively (Figure 3.9). The Ms values measured at body temperature were 62 emu/g and 52 emu/g for MNP and OA-MNP, respectively (Figure 3.10). It was observed that there was a slight decrease in Ms values when the temperature was increased to 37^{o}C. Obtained saturation magnetization values were all below the Ms value of bulk Fe_3O_4 which was reported as 92 emu/g (Tural, Özkan, & Volkan, 2009). The decrease in Ms value of MNP after oleic acid coating could be due to the diamagnetic character of oleic acid.

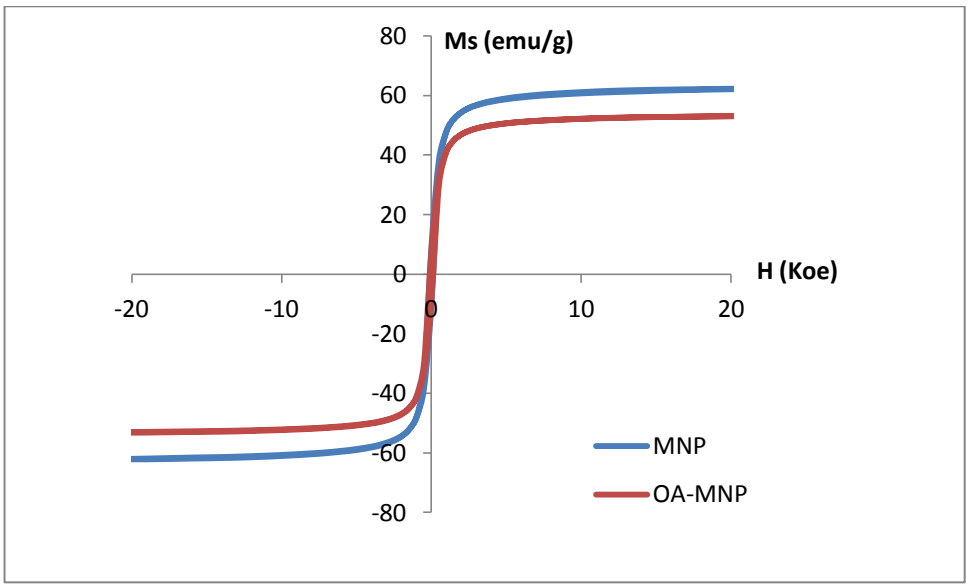

Figure 3.9 M-H curves of MNP and OA-MNP at room temperature (23^{o}C)

Table 3.1 Magnetic properties of MNP and OA-MNP

Sample Name	Ms (emu/g)		Mr (emu/g)		Remanence (Mr/Ms)		Hc (KOe)	
	RT (23^{o}C)	BT (37^{o}C)	RT (23^{o}C)	BT (37^{o})	RT (23^{o}C)	BT (37^{o}C)	RT (23^{o}C)	BT (37^{o}C)
MNP	62	62	9.7	9.1	0.157	0.145	0.107	0.098
OA-MNP	53.13	52.41	8.04	7.54	0.151	0.144	0.105	0.099

M_s : The saturated magnetization, M_r : The residual magnetization, M_r/M_s : The relative saturation remanence, H_c : The coercivity, RT: Room temperature, BT: Body temperature

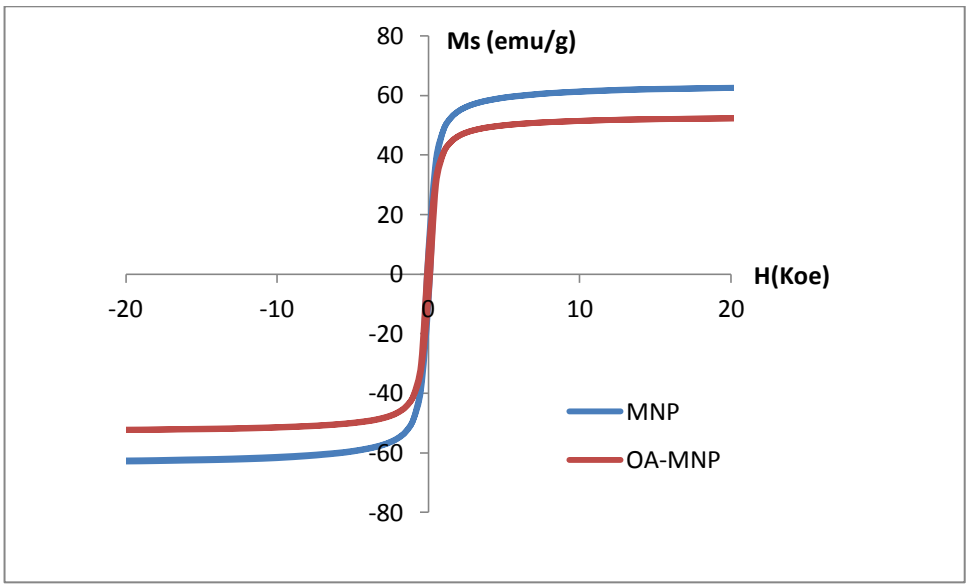

Figure 3.10 M-H curves of MNP and OA-MNP at body temperature (37^{o}C).

These results were consistent with literature. In fact, Liu *et al* reported Ms values of naked and oleic acid coated nanoparticles measured at room temperature as 58 emu/g and 46 emu/g, respectively (X. Liu et al., 2006). According to VSM analysis, MNP and OA-MNP seem to show superparamagnetic characters. In fact, they did not show any hysteresis loop when magnetic field was applied. In addition, they showed negligible remanence and coercivity as indicated in Table 3.1.

Reduced Ms values of OA-MNPs compared to MNPs can be validated by TGA results (Table 3.2). The Ms values of OA-MNP obtained by VSM analysis and calculated by TGA results can be compared. Equation 3.1 shows how to calculate Ms value of oleic acid coated nanoparticles by TGA results (Lan, Liu, Jiang, Zeng, & Wu, 2011). For example, the VSM Ms value of MNP at room

temperature was 62 emu/g. The amount of oleic acid coating and residual MNP core of OA-MNP was found 11% and 89%, respectively (Figure 3.8). When these data were put in Equation 3.1, Ms value of OA-MNP would be calculated as 55 emu/g. Besides, it was found as 52 emu/g by VSM, which shows the correlation between TGA and VSM results.

$$Ms_{TGA} = MS_{VSM}{}^{Fe3O4} \text{ x } \text{(magnetic core \%)} \qquad \text{(Eq. 3.1)}$$

Ms_{TGA} is calculated Ms value of coated MNP based on TGA results,

$MS_{VSM}{}^{Fe3O4}$ is Ms value of coated MNP obtained by VSM analysis,

(magnetic core %) is weight percentage of core MNP in OA-MNP found by TGA .

Table 3.2 Ms (emu/g) values from VSM and TGA

Sample Name	VSM		TGA	
	RT (23^oC)	BT (37^oC)	RT (23^oC)	BT (37^oC)
OA-MNP	53	52	55	55

RT: Room temperature, BT: Body temperature

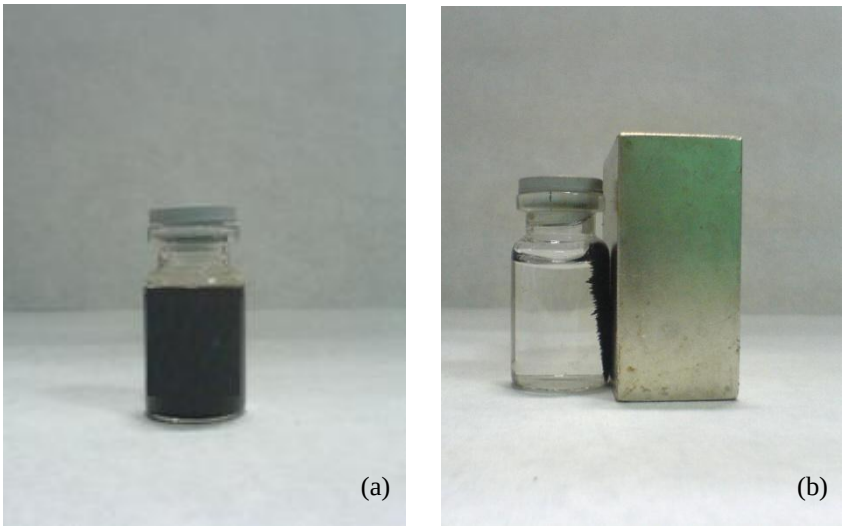

Figure 3.11 Photographs of MNP in water: (a) without external magnetic field and (b) with external magnetic field

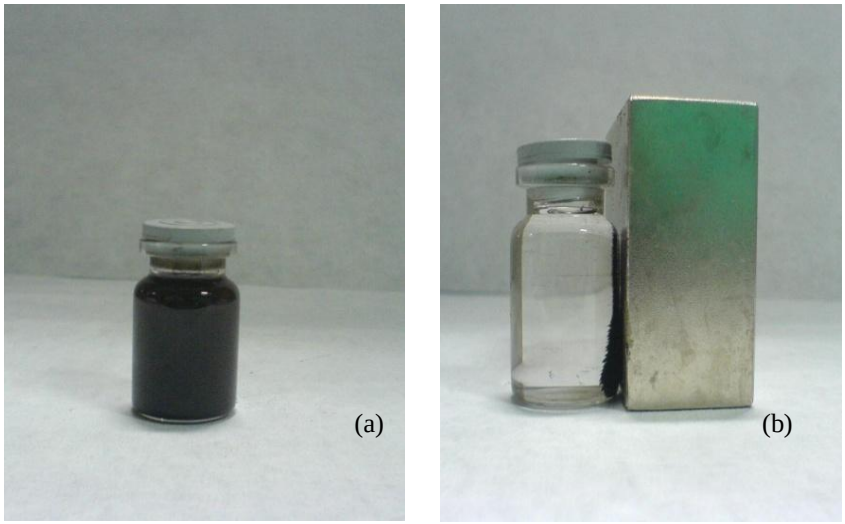

Figure 3.12 Photographs of OA-MNP in DCM : (a) without external magnetic field and (b) with external magnetic field

Magnetic sensitivity of the synthesized nanoparticles were also tested by applying an external magnetic field with a Nd-Fe-B magnet. The bottles containing black suspensions of MNP and OA-MNP are showed in Figure 3.11(a) and Figure 3.12(a), respectively. When the external magnetic field was applied, nanoparticles in the solution were attracted close to the magnets quickly and solution became transparent, as shown in Figure 3.11(b) and Figure 3.12(b). After removal of the external magnetic field, the nanoparticles redispersed in the solution.

3.2 Preparation and Characterization of Magnetic Polymeric Nanoparticles

Oleic acid containing MNPs were coated with PLGA by O/W emulsion-technique. Chemical structure of PLGA-MNP was determined by FTIR spectroscopy. Effects of different OA-MNP (g) / PLGA (g) ratio on magnetite entrapment effciency were investigated through AAS measurements. PLGA-MNP with the highest magnetite entrapment efficiency was characterized with respect to particle morphology, size and magnetic properties by SEM, TEM and VSM measurements.

3.2.1 Fourier Transformed Infrared Spectroscopy

The chemical structures of both PLGA nanoparticles (PLGA-NP) and magnetic PLGA nanoparticles (PLGA-MNP) were determined by FTIR analysis. The characteristic peak of PLGA belonging to C=O bond of ester group was

observed at 1758 cm^{-1} in the spectrum of PLGA-NP, and it shifted to 1755 cm^{-1} in the spectrum of PLGA-MNP (Figure 3.13).

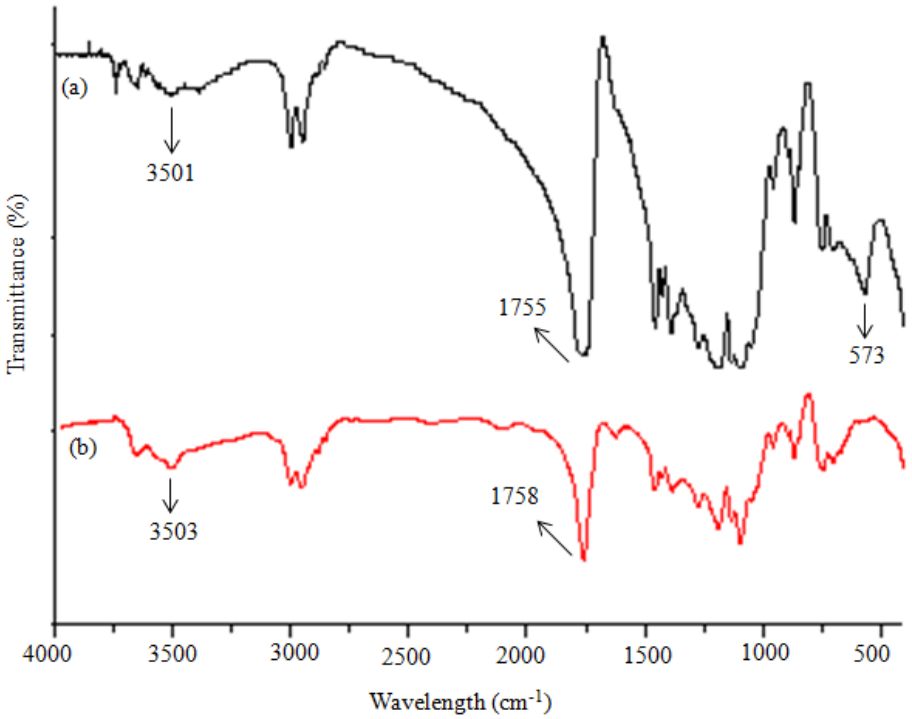

Figure 3.13 FTIR spectra of (a) PLGA-MNP and (b) PLGA-NP

The hydroxyl group of PVA was also confirmed at 3500–3100 cm^{-1} for both samples (Coates & Ed, 2000). The characteristic band of magnetite was present at 570 cm^{-1} in the spectrum of PLGA-MNP (Figure 3.13(a)), but not in the spectrum of PLGA-NP (Figure 3.13(b)).

The peaks around 3000 cm $^{-1}$ most likely belonged to CH_2 stretching mode both from OA-MNP and PLGA (Okassa et al., 2007). These results suggested that magnetic nanoparticles were incorporated into the PLGA polymer .

3.2.2 Atomic Absorption Spectroscopy

Effects of different OA-MNP (g) / PLGA (g) ratios on magnetite entrapment efficiency of prepared polymeric magnetic nanoparticles were investigated through AAS measurements. Briefly, dried OA-MNPs were added with a variable iron oxide/polymer ratio of 1:1, 1:2; 1:4 and 1:8 w/w in polymer coating process.

Magnetite entrapment efficiencies (EE) of prepared PLGA-MNPs were calculated by using equation 2.2 (Table 3.3). Experiments were made duplicate.

Table 3.3 Effect of OA-MNP (g) / PLGA (g) ratio on magnetite entrapment efficiency (%)

OA-MNP(g) / PLGA(g)	**Magnetite EE (%)**
1:1	4±1.20
1:2	8±2.27
1:4	20±3
1:8	63±6.24

The highest magnetite entrapment efficiency was obtained as 63 % (w/w) with iron oxide/polymer ratio of 1:8 (w/w). Its magnetite content, calculated by using equation 2.1, was 7 % (w/w) with a theoretical magnetite loading of 11 % (w/w). It was observed that magnetite entrapment efficiency decreased when the amount of OA-MNP used in the experiment was increased (Table 3.3). This might be due to the iron oxide aggregation (Astete & Sabliov, 2006). In fact, OA-MNPs were exposed to ultrasonication before they were used in emulsion-evaporation process. The duration and power of ultrasonication were the same for all samples. Thus, when they were used in large amounts the power of ultrasonication might have not been enough to disperse them equally. This may result in iron oxide aggregates which cause nonuniform distribution of OA-MNP in the droplet phase of the emulsion. This results in low encapsulation efficiency. Moreover, Raut *et al* mention that utilization of dried OA-MNP in emulsion-evaporation process instead of wet precipitate of OA-MNP, could lead to formation of aggregates which might be resulted from the partial desorption of oleic acid from the surface of OA-MNP. This may lead to low encapsulation efficiency results (Raut, Kirthivasan, Bommana, Squillante, & Sadoqi, 2010).

Wassel *et al* mention that 8% (w/w) magnetite in PLGA is sufficient to move the particles to a specific location in guinea pig (Wassel, Grady, Kopke, & Dormer, 2007). This reveals that obtained PLGA-MNP with magnetite content close to 8% may have potential targeting ability.

3.2.3 Scanning Electron Microscopy

SEM images of PLGA-MNP show that polymeric nanoparticles were spherical in shape (Figure 3.14).

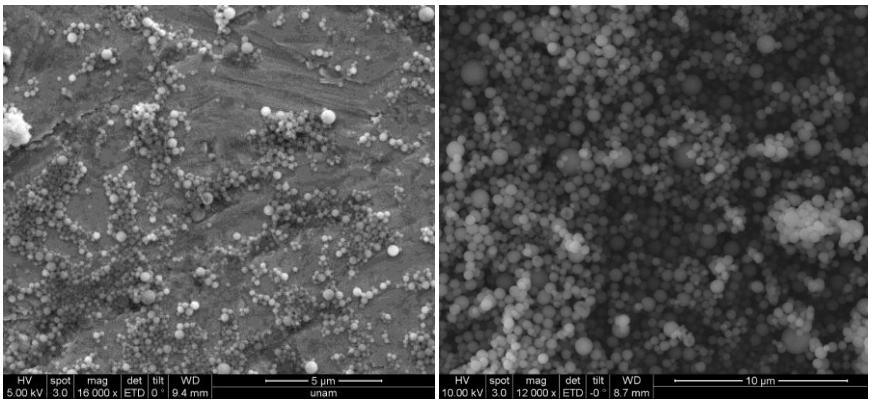

Figure 3.14 SEM images of PLGA-MNP

3.2.4 Transmission Electron Microscopy

The results of TEM obtained for PLGA-MNP indicated that polymer coated nanoparticles were uniform in shape and size (Figure 3.15). In addition, the core–shell structure of the PLGA-MNP could be clearly seen. In fact, the size of magnetite core was approximately 10 nm, and total size of nanoparticle was around 65 nm after polymer coating.

It is noteworthy to mention that the particles obtained were within the critical limits of size for drug delivery applications which were between 10 and 100 nm (Arruebo et al., 2007).

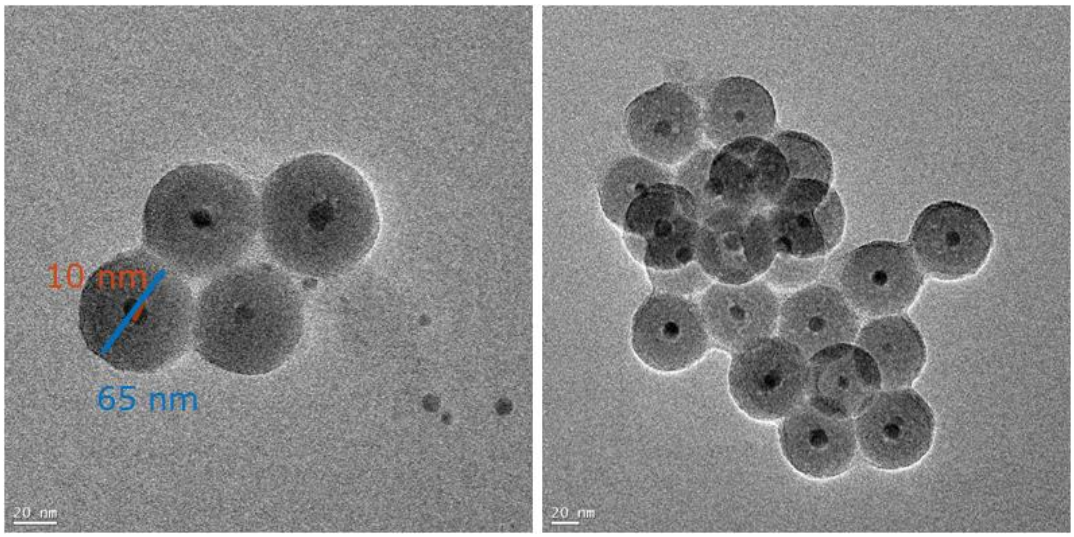

Figure 3.15 TEM images of PLGA-MNP

3.2.5 Vibration Sample Magnetometer Analysis

Magnetic characteristics of PLGA-MNP was determined by VSM analysis at both room temperature (23^{o}C) and body temperature (37^{o}C) (Figure 3.16). The obtained Ms values were 4,32 and 4,14 emu/g for measurements in room temperature and body temperature, respectively. Magnetic properties of PLGA-MNP was given in Table 3.4. A significant drop in Ms value was observed after nanoparticles were coated with polymer. This decrease could be related to the polymer coating contributing as a non-magnetic mass to the total sample volume. Despite this decrease, PLGA-MNP could still quickly respond to

external magnetic field and move toward Nd-Fe-B magnet. Moreover, it is mentioned in the literature that Fe-based nanoparticles with a size of less than 25 nm show superparamagnetic behavior (Arruebo et al., 2007). In fact, the size of the magnetic core in PLGA-MNP was around 10 nm which was in the optimum size range for superparamagnetism. In addition, polymeric magnetic nanoparticles did not show any hysteresis loop at both temperatures with inconsiderable Mr and Hc. Obtained Ms values were higher than previously reported results (Lee et al., 2005). According to VSM results, PLGA coated magnetic nanoparticles seem to be superparamagnetic.

Magnetic saturation decrease observed with VSM was validated by using the Equation 3.1, considering the magnetite content calculated by AAS results (Section 3.2.2).

Table 3.4 Magnetic properties of PLGA-MNP

Sample Name	Ms (emu/g)		Mr (emu/g)		Remanence (Mr/Ms)		Hc (KOe)	
	RT (23^{o}C)	BT (37^{o}C)	RT (23^{o}C)	BT (37^{o}C)	RT (23^{o}C)	BT (37^{o}C)	RT (23^{o}C)	BT (37^{o}C)
PLGA-MNP	4.32	4.14	0.7	0.15	0.16	0.036	0.11	0.07

M_s : The saturated magnetization, M_r : The residual magnetization, M_r/M_s : The relative saturation remanence, H_c : The coercivity, RT: Room temperature, BT: Body temperature

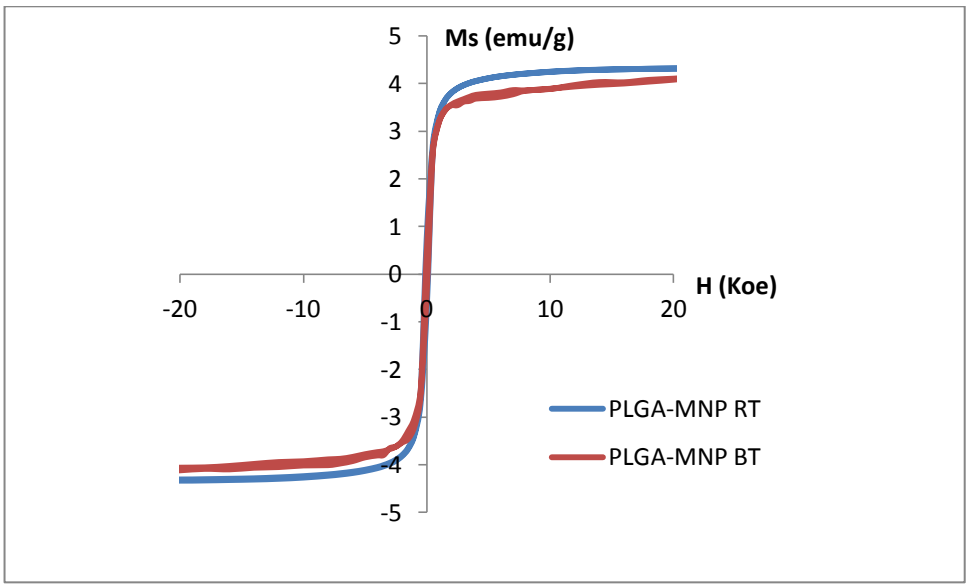

Figure 3.16 M-H curves of PLGA-MNP at both room temperature (23 ^{o}C) and body temperature (37^{o}C)

Table 3.5 Ms (emu/g) values from VSM and AAS.

Sample Name	VSM		AAS	
	RT (23^{o}C)	BT (37^{o}C)	RT (23^{o}C)	BT (37^{o}C)
PLGA-MNP	4.32	4.14	4.34	4.34

RT: Room temperature, BT: Body temperature

3.3 Preparation and Characterization of Drug Loaded Magnetic Polymeric Nanoparticles

Doxorubicin loaded magnetic polymeric nanoparticles (DOX-PLGA-MNP) were prepared by o/w emulsion evaporation method. Incorporation of doxorubicin in PLGA was confirmed with UV-Vis absorption spectra. Morphology of obtained drug loaded nanoparticles were observed via SEM and preliminary drug extraction studies were performed.

3.3.1 UV-Vis Absorption Spectroscopy

UV-Vis absorption spectra measurements between 400 and 800 nm wavelengths were performed to confirm the encapsulation of DOX by PLGA.

As shown in Figure 3.17, doxorubicin loaded magnetic polymeric nanoparticles (DOX-PLGA-MNP) dissolved in DMSO gave peak at 480 nm whereas unloaded PLGA-MNPs did not, which reveals the presence of doxorubicin in prepared magnetic polymeric nanoparticles.

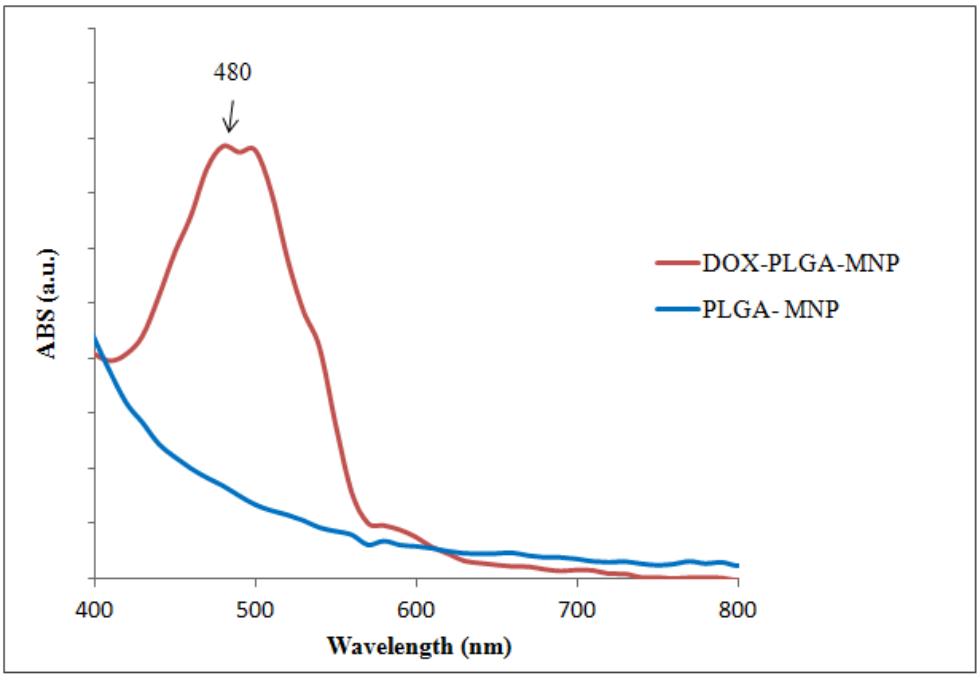

Figure 3.17 UV-Vis absorption spectra of DOX-PLGA-MNP and PLGA-MNP dissolved in DMSO

3.3.2 Preliminary Drug Extraction Studies

As a preliminary drug extraction study, a calibration curve of standard doxorubicin solution in DMSO was prepared to determine the doxorubicin concentration extracted from DOX-PLGA-MNP. As shown in Figure 3.18, calibration curve was linear over studied range with a correlation coefficient of $R^2 = 0.9956$. The amount of doxorubicin extracted from DOX-MNP in 3 hours was calculated as 5.8 ±0.8 µg/ml. This study was performed in 3 hours to determine the drug extraction behavior of DOX-PLGA-MNP. Besides, in order to exactly estimate the total drug content of DOX-PLGA-MNP, drug extraction studies could be performed in an extended period of time. Obtained result

indicates that prepared drug loaded magnetic polymeric nanoparticles had an efficient design which enables drug extraction from polymer coating. In addition, due to presence of doxorubicin in DOX-PLGA-MNP, a significant cell death was observed in cytotoxicity studies of DOX-PLGA-MNP (Figure 3.21). This study may have potential contribution for future studies about estimating drug content and drug loading efficiency.

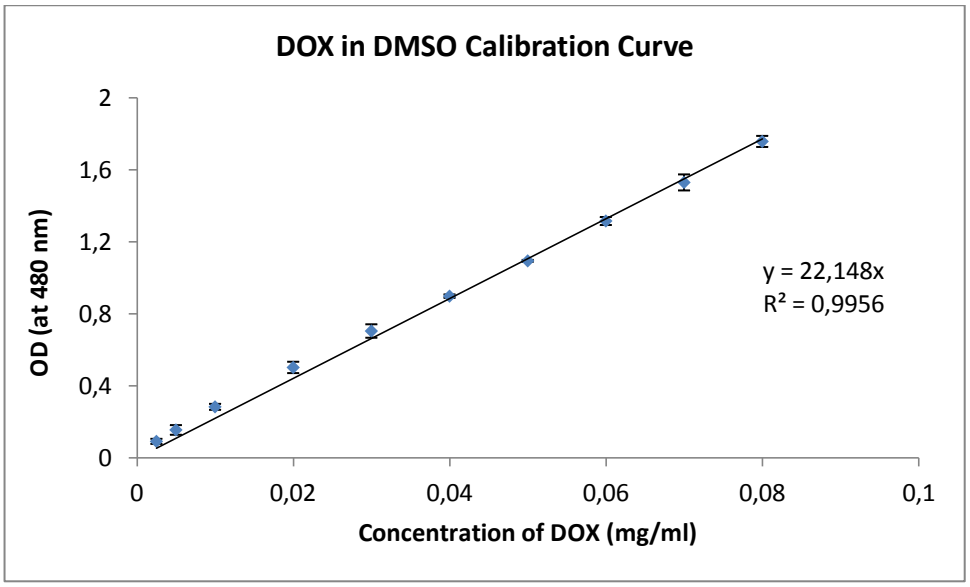

Figure 3.18 Calibration curve of doxorubicin dissolved in DMSO

3.3.3 Scanning Electron Microscopy

Morphology of DOX-PLGA-MNP was observed with SEM examinations. It was observed that nanoparticles are in spherical shape (Figure 3.19).

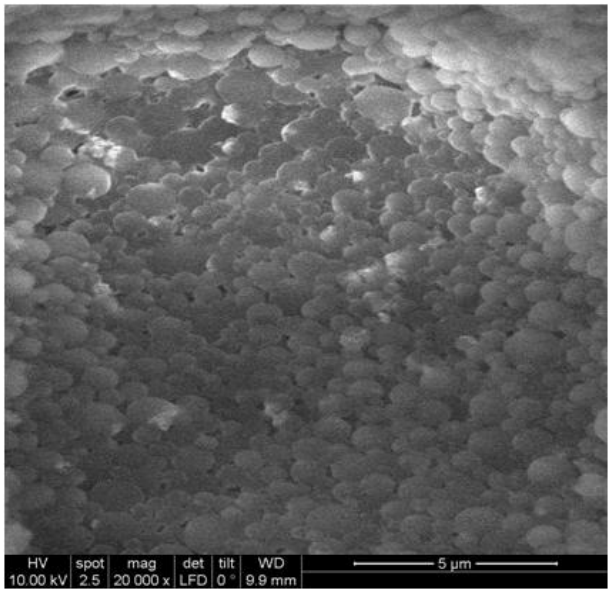

Figure 3.19 SEM image of DOX-PLGA-MNP

3.4 Cell Proliferation Assay

XTT cell proliferation assay was used to evaluate the cytotoxicity of prepared nanoparticles *in vitro* by using MCF-7 cells. Cells were incubated with nanoparticles for 72 h. The detailed procedure was explained in Section 2.2.6.6.

Figure 3.20 indicates the cell proliferation profiles of MCF-7 cells incubated with MNP, PLGA-NP, and PLGA-MNP at maximum exposure dosage of 500 μg ml^{-1}. It was observed that MNP did not show any significant toxicity to cells in the range of 2-125 μg ml^{-1}. Although, it had significant cytotoxicity at concentrations of both 250 and 500 μg ml^{-1}, cell proliferation was reduced just only to 77 %. Gupta *et al.* also reported that naked superparamagnetic iron oxide nanoparticles showed significant cytotoxicity at high concentrations (Gupta & Wells, 2004). Viability of cells incubated with PLGA-NP remained at about 90 % relative to untreated cells, briefly they were not cytotoxic to the cells. This was an expected result because PLGA is biocompatible and its degradation products do not cause toxic effects to cells (Şen, 2009).

PLGA-MNP showed similar results with empty nanoparticles (PLGA-NP) up to 250 μg ml^{-1}. This reveals that Fe_3O_4 nanoparticles incorporated in polymeric nanoparticles did not cause significant cytotoxicity on MCF-7 cells. A significant cytotoxicity observed at 500 μg ml^{-1} but cell proliferation was up to 87 %.

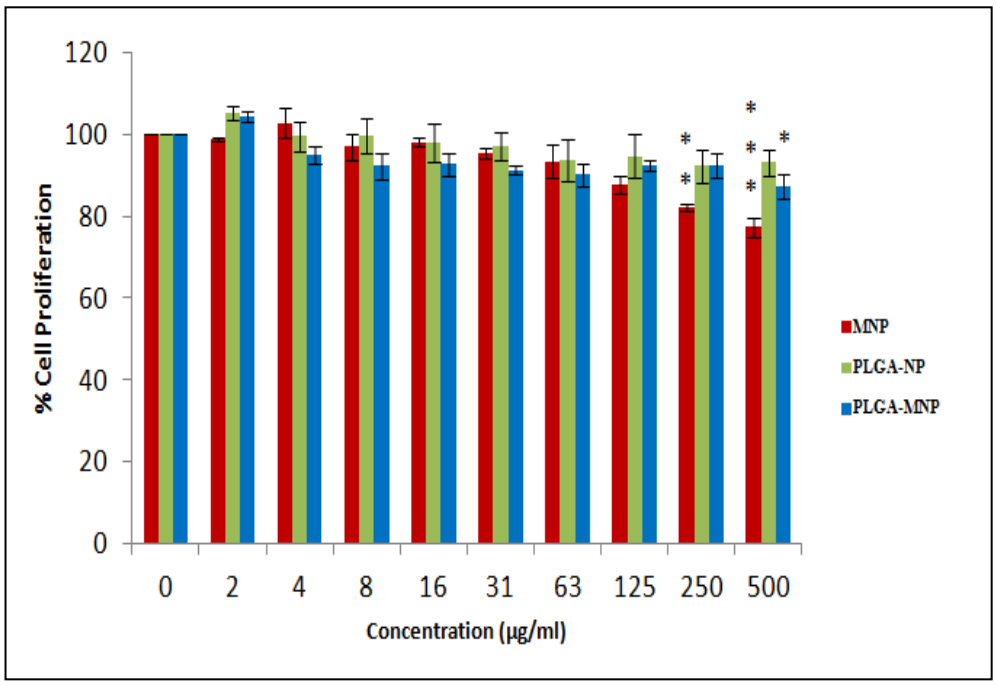

Figure 3.20 MCF-7 cell proliferation profiles after incubation with MNP, PLGA-NP and PLGA-MNP. All experiments were carried out in triplicates. *p<0.05, **p<0.01, ***p<0.001 compared to nanoparticle untreated cells which are assumed to show 100% cell proliferation (control group). Results were given as Mean ± SEM.

In addition to these results, a non significant increase in the cell viability is observed commonly for all nanoparticles in the concentration of 2 µg ml^{-1} which needs to be elucidated. Examples of this phenomenon are also in the literature (Ankamwar et al., 2010; Gupta & Wells, 2004).

Results showed that obtained nanoparticles could be used for in vitro studies.

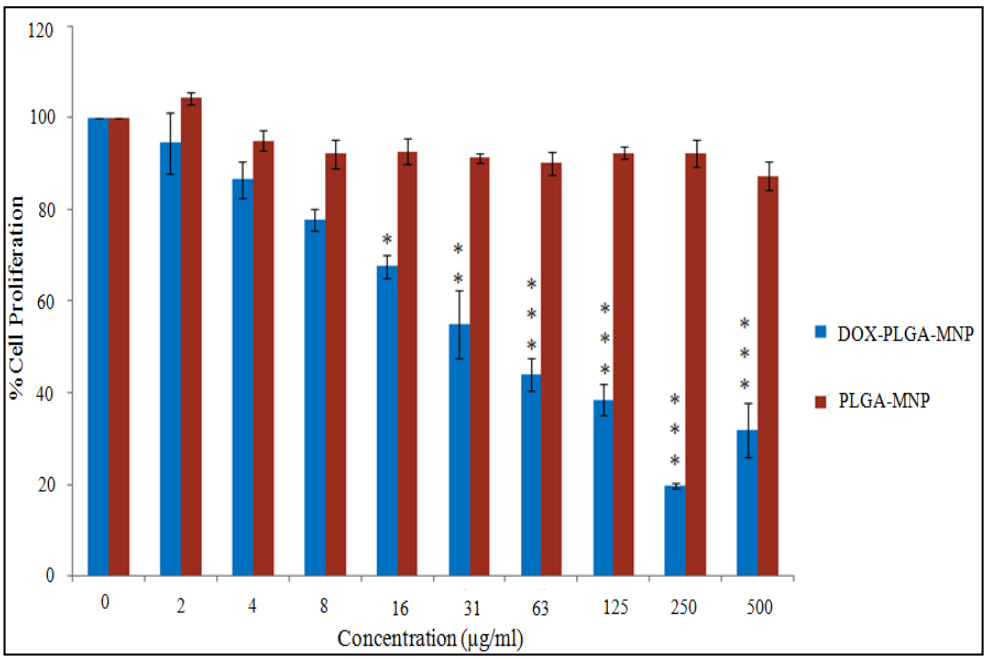

Figure 3.21 MCF-7 cell proliferation profiles after incubation with PLGA-MNP and DOX-PLGA-MNP. Experiments were carried out in triplicates. *p<0.05, **p<0.01 and ***p<0.001 compared to PLGA-MNP. Results were given as Mean ± SEM.

In order to investigate whether doxorubicin encapsulated PLGA have cytototoxic effects on MCF-7 cells, DOX-PLGA-MNP was given to cells at the maximum exposure dosage of 500 µg ml^{-1}. Cell proliferation was compared with PLGA-MNP and results showed that DOX-PLGA-MNP lead to significant cell death in the range of 16 and 500 µg ml^{-1}. The cell proliferations were found as 20 % and 32 % at concentrations of 250 and 500 µg ml^{-1}, respectively (Figure 3.21). Compared to PLGA-MNP, the huge reduce in cell proliferation might be due to antiproliferative effect of doxorubicin loaded in polymer.

CHAPTER 4

CONCLUSION

Magnetic nanoparticles are used in targeted drug delivery studies owing to their wide range of chemical, physical and magnetic properties. When these nanoparticles are coated with biocompatible polymers, they may act as a promising drug carriers and may be used in targeted drug delivery applications. In this study, magnetic nanoparticles (MNP) were synthesized and it was found that they had a characteristic cubic crystal structure of Fe_3O_4. Then they were covered with oleic acid (OA-MNP) and hydrophobicity of OA-MNPs were proved. The weight ratio of oleic acid coat on OA-MNP was found 11%. OA-MNPs were encapsulated into PLGA. Adjusting parameters provided efficient ways to increase the magnetite entrapment efficiency. The highest magnetite entrapment efficiency was estimated as 63%. Size and surface characterization studies showed that prepared PLGA-MNPs had uniform size in between the size range of nanoparticles which are used in biomedical applications. Synthesized nanoparticles seem to be superparamagnetic. Cytotoxicity of obtained nanoparticles were investigated by using MCF-7 cells in vitro. Moreover, anticancer drug doxorubicin was loaded to PLGA-MNP. Besides, cytotoxicity of drug loaded magnetic polymeric nanoparticles was investigated. DOX-PLGA-MNP had a significant toxicity on cells compared to nanoparticles without drug.

These results demonstrated that due to their appropriate size, noncytotoxic, and superparamagnetic characters, prepared PLGA coated magnetic nanoparticles may be suitable for targeted drug delivery applications and the data obtained from drug studies may contribute to future drug delivery researches.

REFERENCES

Acharya, S., & Sahoo, S. K. (2011). PLGA nanoparticles containing various anticancer agents and tumour delivery by EPR effect. *Advanced Drug Delivery Reviews*, *63*(3), 170-83. Elsevier B.V. doi:10.1016/j.addr.2010.10.008

American Cancer Society, (2012). Cancer Facts & Figures. Retrieved January 4, 2012, from http://www.cancer.org /acs/groups/content/@epidemiologysurveilance/documents/document/acspc-031941.pdf

Andhariya, N., Chudasama, B., Mehta, R. V., & Upadhyay, R. V. (2010). Biodegradable thermoresponsive polymeric magnetic nanoparticles: a new drug delivery platform for doxorubicin. *Journal of Nanoparticle Research*, *13*(4), 1677-1688. doi:10.1007/s11051-010-9921-6

Ankamwar, B., Lai, T. C., Huang, J. H., Liu, R. S., Hsiao, M., Chen, C. H., & Hwu, Y. K. (2010). Biocompatibility of Fe(3)O(4) nanoparticles evaluated by in vitro cytotoxicity assays using normal, glia and breast cancer cells. *Nanotechnology*, *21*(7), 75102. doi:10.1088/0957-4484/21/7/075102

Arias, J. L., Gallardo, V., Gómez-Lopera, S. a, Plaza, R. C., & Delgado, a V. (2001). Synthesis and characterization of poly(ethyl-2-cyanoacrylate) nanoparticles with a magnetic core. *Journal of Controlled Release : Official Journal of the Controlled Release Society*, *77*(3), 309-21.

Arruebo, M., Fernández-pacheco, R., Ibarra, M. R., & Santamaría, J. (2007). Magnetic nanoparticles: Controlled release of drugs from nanostructured functional materials. *Review Literature and Arts of the Americas*, *2*(3), 22-32.

Astete, C. E., Kumar, C. S. S. R., & Sabliov, C. M. (2007). Size control of poly(d,l-lactide-co-glycolide) and poly(d,l-lactide-co-glycolide)-magnetite nanoparticles synthesized by emulsion evaporation technique. *Colloids and Surfaces A: Physicochemical and Engineering Aspects*, *299*(1-3), 209-216. doi:10.1016/j.colsurfa.2006.11.055

Astete, C., & Sabliov, C. (2006). Synthesis of Poly(DL-Lactide-Co-Glycolide) Nanoparticles with Entrapped Magnetite by Emulsion Evaporation Method. *Particulate Science and Technology*, *24*(3), 321-328. doi:10.1080/02726350600840696

Balogh, L. P. (2007). Dendrimer 101. *Advances in Experimental Medicine and Biology*, *620*, 136-55.

Berry, C. C., & Curtis, A. S. G. (2003). Functionalisation of magnetic nanoparticles for applications in biomedicine. *Journal of Physics D: Applied Physics*, *36*(13), R198-R206. doi:10.1088/0022-3727/36/13/203

Bhosle, J., & Hall, G. (2009). Principles of cancer treatment by chemotherapy. *Surgery (Oxford)*, *27*(4), 173-177. doi:10.1016/j.mpsur.2009.01.006

Bisht, S., & Maitra, A. (2009). Nanoparticles for Solid Tumor. *Cancer*, 415-425. doi:10.1002/wnan.043

Can, M. M. (2005). *Investigation of physical properties of magnetic nanoparticles* (MSc Thesis, Hacettepe University).

Cell Proliferation Assay with XTT Reagent Protocol. Biological Industries. Retrieved September 24, 2011, from http://www.bioind.com/htmls/article.aspx?c0=12557&bsp=13275

Cho, K., Wang, X., Nie, S., Chen, Z. G., & Shin, D. M. (2008). Therapeutic nanoparticles for drug delivery in cancer. *Clinical Cancer Research : An Official Journal of the American Association for Cancer Research*, *14*(5), 1310-6. doi:10.1158/1078-0432.CCR-07-1441

Chomoucka, J., Drbohlavova, J., Huska, D., Adam, V., Kizek, R., & Hubalek, J. (2010). Magnetic nanoparticles and targeted drug delivering. *Pharmacological Research : The Official Journal of the Italian Pharmacological Society*, *62*(2), 144-9. Elsevier Ltd. doi:10.1016/j.phrs.2010.01.014

Coates, J., & Ed, R. A. M. (2000). Interpretation of Infrared Spectra , A Practical Approach Interpretation of Infrared Spectra , A Practical Approach. *Interpretation a Journal of Bible and Theology*, 10815-10837.

Coley, H. M. (2008). Mechanisms and strategies to overcome chemotherapy resistance in metastatic breast cancer. *Cancer Treatment Reviews*, *34*(4), 378-90. doi:10.1016/j.ctrv.2008.01.007

Danhier, F., Feron, O., & Préat, V. (2010). To exploit the tumor microenvironment: Passive and active tumor targeting of nanocarriers for anti-cancer drug delivery. *Journal of Controlled Release : Official Journal of the Controlled Release Society*, *148*(2), 135-46. Elsevier B.V. doi:10.1016/j.jconrel.2010.08.027

Doxorubicin PI. (2003). Retrieved October 20, 2011, from http://www.accessdata.fda.gov/drugsatfda_docs/label/2003/050467s068lbl.pdf

Douziech-Eyrolles, Laurence, Marchais, H., Hervé, K., Munnier, E., Soucé, M., Linassier, C., Dubois, P., et al. (2007). Nanovectors for anticancer agents based on superparamagnetic iron oxide nanoparticles. *International Journal of Nanomedicine*, *2*(4), 541-50.

Dönmez, Y. (2010). Reversal of multidrug resistance by small interfering rnas (sirna) in doxorubicin resistant MCF-7 breast cancer cells (MSc Thesis, METU).

Eken, A. E. (2008). *Characterization of magnetite thin films produced by sol-gel processing* (MSc Thesis, METU). Retrieved from http://etd.lib.metu.edu.tr/upload/12609298/index.pdf

Epherre, R., Goglio, G., Mornet, S. & Duguet, E. (2011). Hybrid magnetic nanoparticles for drug delivery. *Comprehensive Biomaterials*, 4, 575-593 http://dx.doi.org/10.1016/B978-0-08-055294-1.00145-8

Gossuin, Y., Gillis, P., Hocq, A., Vuong, Q. L., & Roch, A. (2009). Magnetic resonance relaxation properties of superparamagnetic particles. *Molecular Imaging*. doi:10.1002/wnan.036

Gou, M. L., Qian, Z. Y., Wang, H., Tang, Y. B., Huang, M. J., Kan, B., Wen, Y. J., et al. (2008). Preparation and characterization of magnetic poly (epsilon-caprolactone)-poly (ethyleneglycol) - poly (epsilon-caprolactone) microspheres. *Journal of Materials Science. Materials in Medicine*, *19*(3), 1033-41. doi:10.1007/s10856-007-3230-3

Gupta, A. K., & Gupta, M. (2005). Synthesis and surface engineering of iron oxide nanoparticles for biomedical applications. *Biomaterials*, *26*(18), 3995-4021. doi:10.1016/j.biomaterials.2004.10.012

Gupta, A. K., & Wells, S. (2004). Surface-modified superparamagnetic nanoparticles for drug delivery: preparation, characterization, and cytotoxicity studies. *IEEE Transactions on Nanobioscience*, *3*(1), 66-73.

Güç, E. (2008). *Synthesis and characterization of fatty acid based hyperbranched polymers for anti-cancer drug delivery* (MSc Thesis, METU).

Hans, M. L., & Lowman, A. M. (2002). Biodegradable nanoparticles for drug delivery and targeting. *Journal of Controlled Release*, 6, 319-327.

Jain, T. K., Richey, J., Strand, M., Leslie-Pelecky, D. L., Flask, C. a, & Labhasetwar, V. (2008). Magnetic nanoparticles with dual functional properties: drug delivery and magnetic resonance imaging. *Biomaterials*, *29*(29), 4012-21. doi:10.1016/j.biomaterials.2008.07.004

Kumar, A., Jena, P. K., Behera, S., Lockey, R. F., Mohapatra, S., & Mohapatra, S. (2010). Multifunctional magnetic nanoparticles for targeted delivery. *Nanomedicine : Nanotechnology, Biology, and Medicine*, *6*(1), 64-9. Elsevier Inc. doi:10.1016/j.nano.2009.04.002

Lan, F., Liu, K.-xia, Jiang, W., Zeng, X.-bo, & Wu, Y. (2011). Facile synthesis of monodisperse superparamagnetic Fe(3)O(4) / PMMA composite nanospheres with high magnetization. *Nanotechnology; 22(22): 225604*. doi:10.1088/0957-4484/22/22/225604

Lee, S.-J., Jeong, J.-R., Shin, S.-C., Kim, J.-C., Chang, Y.-H., Lee, K.-H., & Kim, J.-D. (2005). Magnetic enhancement of iron oxide nanoparticles encapsulated with poly(d,l-lactide-co-glycolide). *Colloids and Surfaces A: Physicochemical and Engineering Aspects*, *255*(1-3), 19-25. doi:10.1016/j.colsurfa.2004.12.019

Leonard, R. C. F., Williams, S., Tulpule, A., Levine, A. M., & Oliveros, S. (2009). Improving the therapeutic index of anthracycline chemotherapy : Focus on liposomal doxorubicin (Myocet^{TM}). *Seminars in Oncology*, *18*, 218-224. doi:10.1016/j.breast.2009.05.004

Liu, X., Kaminski, M., Guan, Y., Chen, H., Liu, H., & Rosengart, a. (2006). Preparation and characterization of hydrophobic superparamagnetic magnetite gel. *Journal of Magnetism and Magnetic Materials*, *306*(2), 248-253. doi:10.1016/j.jmmm.2006.03.049

Mahmoudi, M., Sant, S., Wang, B., Laurent, S., & Sen, T. (2011). Superparamagnetic iron oxide nanoparticles (SPIONs): development, surface modification and applications in chemotherapy. *Advanced Drug Delivery Reviews*, *63*(1-2), 24-46. Elsevier B.V. doi:10.1016/j.addr.2010.05.006

McBain, S. C., Yiu, H. H. P., & Dobson, J. (2008). Magnetic nanoparticles for gene and drug delivery. *International Journal of Nanomedicine*, *3*(2), 169-80.

Mishra, B., Patel, B. B., & Tiwari, S. (2010). Colloidal nanocarriers: a review on formulation technology, types and applications toward targeted drug delivery. *Nanomedicine : Nanotechnology, Biology, and Medicine*, *6*(1), 9-24. Elsevier Inc. doi:10.1016/j.nano.2009.04.008

Muthu, M. (2009). Nanoparticles based on PLGA and its co-polymer: An overview. *Asian Journal of Pharmaceutics*, *3*(4), 266. doi:10.4103/0973-8398.59948

Narod, S. a. (2011). Screening of women at high risk for breast cancer. *Preventive Medicine*, *53*(3), 127-30. Elsevier Inc. doi:10.1016/j.ypmed.2011.06.017

Okassa, L. N., Marchais, H., Douziech-Eyrolles, L., Hervé, K., Cohen-Jonathan, S., Munnier, E., Soucé, M., et al. (2007). Optimization of iron oxide nanoparticles encapsulation within poly(d,l-lactide-co-glycolide) sub-micron particles. *European Journal of Pharmaceutics and Biopharmaceutics : Official Journal of Arbeitsgemeinschaft für Pharmazeutische Verfahrenstechnik e.V*, *67*(1), 31-8. doi:10.1016/j.ejpb.2006.12.020

Park, J. H., Lee, S., Kim, J.-H., Park, K., Kim, K., & Kwon, I. C. (2008). Polymeric nanomedicine for cancer therapy. *Progress in Polymer Science*, *33*(1), 113-137. doi:10.1016/j.progpolymsci.2007.09.003

Pelengaris, S. & Khan, M. (2006). *The Molecular Biology of Cancer* (pp. 7, 8). Malden, MA ; Oxford : Blackwell

Praetorius, N. P., & Mandal, T. K. (2007). Engineered Nanoparticles in Cancer Therapy. *Science*, 37-51.

Raut, S. L., Kirthivasan, B., Bommana, M. M., Squillante, E., & Sadoqi, M. (2010). The formulation, characterization and in vivo evaluation of a magnetic carrier for brain delivery of NIR dye. *Nanotechnology*, *21*, *395102*. doi:10.1088/0957-4484/21/39/395102

Ruddon, R. W. (2007). Characteristics of human cancer. *Cancer Biology* (4th ed., pp. 4, 7). New York : Oxford University Press.

Sinha, R., Kim, G. J., Nie, S., & Shin, D. M. (2006). Nanotechnology in cancer therapeutics: bioconjugated nanoparticles for drug delivery. *Molecular Cancer Therapeutics*, *5*(8), 1909-17. doi:10.1158/1535-7163.MCT-06-0141

Sun, C., Lee, J. S. H., & Zhang, M. (2008). Magnetic nanoparticles in MR imaging and drug delivery. *Advanced Drug Delivery Reviews*, *60*(11), 1252-65. doi:10.1016/j.addr.2008.03.018

Şen, G. P. (2009). *Poly (Dl-Lactic-Co-Glycolic Acid) microparticles and synthetic peptide drug conjugate for anti-cancer drug delivery* (MSc Thesis, METU). Retrieved October 23, 2011 from http://etd.lib.metu.edu.tr/upload/12611405/index.pdf

Tewes, F., Munnier, E., Antoon, B., Ngaboni Okassa, L., Cohen-Jonathan, S., Marchais, H., Douziech-Eyrolles, L., et al. (2007). Comparative study of doxorubicin-loaded poly(lactide-co-glycolide) nanoparticles prepared by single and double emulsion methods. *European Journal of Pharmaceutics and Biopharmaceutics : Official Journal of Arbeitsgemeinschaft für Pharmazeutische Verfahrenstechnik e.V*, *66*(3), 488-92. doi:10.1016/j.ejpb.2007.02.016

The National Cancer Institute, (2011). Breast Cancer. Retrieved October 12, 2011, from http://cancer.gov/cancertopics/types/breast

Tucker, J. M., & Rizk, B. (2011). Hereditary female cancers: Breast, ovarian, and endometrial. *Middle East Fertility Society Journal*, *16*(4), 241-247. Middle East Fertility Society. doi:10.1016/j.mefs.2010.12.003

Tuncer, M. (Ed.) (2010). *Cancer Report 2010* (pp. 21, 415, 416). Ankara : New Hope in Health Foundation

Tural, B., Özkan, N., & Volkan, M. (2009). Preparation and characterization of polymer coated superparamagnetic magnetite nanoparticle agglomerates. *Journal of Physics and Chemistry of Solids*, *70*(5), 860-866. doi:10.1016/j.jpcs.2009.04.007

Turton, R. (2000). Magnetic properties. *The Physics of Solids* (pp. 215-218). New York : Oxford University Press.

Veiseh, O., Gunn, J. W., & Zhang, M. (2010). Design and fabrication of magnetic nanoparticles for targeted drug delivery and imaging. *Advanced Drug Delivery Reviews*, *62*(3), 284-304. Elsevier B.V. doi:10.1016/j.addr.2009.11.002

Washbrook, E. (2006). Risk factors and epidemiology of breast cancer. *Women's Health Medicine*, *3*(1), 8-14. doi:10.1383/wohm.2006.3.1.8

Wassel, R. a., Grady, B., Kopke, R. D., & Dormer, K. J. (2007). Dispersion of superparamagnetic iron oxide nanoparticles in poly(d,l-lactide-co-glycolide) microparticles. *Colloids and Surfaces A: Physicochemical and Engineering Aspects*, *292*(2-3), 125-130. doi:10.1016/j.colsurfa.2006.06.012

Wuang, S. C., Neoh, K. G., Kang, E.-T., Pack, D. W., & Leckband, D. E. (2007). Synthesis and functionalization of polypyrrole-Fe(3)O(4) nanoparticles for applications in biomedicine. *Journal of Materials Chemistry*, *17*(31), 3354. doi:10.1039/b702983g

Yang, J., Park, S.-B., Yoon, H.-G., Huh, Y.-M., & Haam, S. (2006, November 6). Preparation of poly epsilon-caprolactone nanoparticles containing magnetite for magnetic drug carrier. *International Journal of Pharmaceutics*. doi:10.1016/j.ijpharm.2006.06.029

Yang, K., Peng, H., Wen, Y., & Li, N. (2010). Re-examination of characteristic FTIR spectrum of secondary layer in bilayer oleic acid-coated Fe(3)O(4) nanoparticles. *Applied Surface Science*, *256*(10), 3093-3097. doi:10.1016/j.apsusc.2009.11.079

Zeng, J., Yang, L., Liang, Q., Zhang, X., Guan, H., Xu, X., Chen, X., et al. (2005). Influence of the drug compatibility with polymer solution on the release kinetics of electrospun fiber formulation. *Journal of Controlled Release : Official Journal of the Controlled Release Society*, *105*(1-2), 43-51. doi:10.1016/j.jconrel.2005.02.024

Zhang, L., He, R., & Gu, H. (2006). Oleic acid coating on the monodisperse magnetite nanoparticles. *Applied Surface Science*, *253*(5), 2611-2617. doi:10.1016/j.apsusc.2006.05.023

Zhang, Y. & Chatterjee D.K. (2006). Liposomes, dendrimers and other polymeric nanoparticles for targeted delivery of anticancer agents-A comparative study. In C.S.S.R. Kumar (Ed.), *Nanoparticles for cancer therapy* (p. 341). Weinheim: Wiley-VCH.

APPENDIX A

EXPERIMENTAL *d* (Å) SPACINGS

Experimental *d* spacings calculated from the XRD patterns and standard data from ICDD (The International Centre for Diffraction Data) cards are listed in Table A.1.

Table A.1 Experimental and standard *d* (Å) spacings with their respective diffracting plane indices (*hkl)*.

***d*(Exp)**	***d* (Fe_3O_4)**	***hkl* indices**
2.959	2.967	220
2.525	2.532	311
2.097	2.099	400
1.708	1.714	422
1.613	1.615	511
1.480	1.484	440